

RESEARCH ARTICLE

10.1002/2014JD022784

Key Points:

- We examine trends and variability in U.S. surface ozone for each season
- Emission changes decrease East U.S. summer O₃ and amplitude of the annual cycle
- Strong correlation of observed and modeled surface O₃ IAV in summer

Supporting Information:

- Figures S1–S5
- Table S1
- Table S2

Correspondence to:

S. A. Strode,
sarah.a.strode@nasa.gov

Citation:

Strode, S. A., J. M. Rodriguez, J. A. Logan, O. R. Cooper, J. C. Witte, L. N. Lamsal, M. Damon, B. Van Aartsen, S. D. Steenrod, and S. E. Strahan (2015), Trends and variability in surface ozone over the United States, *J. Geophys. Res. Atmos.*, 120, 9020–9042, doi:10.1002/2014JD022784.

Received 30 OCT 2014

Accepted 9 AUG 2015

Accepted article online 13 AUG 2015

Published online 14 SEP 2015

Trends and variability in surface ozone over the United States

Sarah A. Strode^{1,2}, Jose M. Rodriguez², Jennifer A. Logan³, Owen R. Cooper^{4,5}, Jacquelyn C. Witte^{2,6}, Lok N. Lamsal^{1,2}, Megan Damon^{2,6}, Bruce Van Aartsen^{2,6}, Stephen D. Steenrod^{1,2}, and Susan E. Strahan^{1,2}

¹Universities Space Research Association, Columbia, Maryland, USA, ²NASA Goddard Space Flight Center, Greenbelt, Maryland, USA, ³School of Engineering and Applied Science, Harvard University, Cambridge, Massachusetts, USA, ⁴Cooperative Institute for Research in Environmental Sciences, University of Colorado, Boulder, Colorado, USA, ⁵NOAA Earth System Research Laboratory, Boulder, Colorado, USA, ⁶Science Systems and Applications Inc., Lanham, Maryland, USA

Abstract We investigate the observed trends and interannual variability in surface ozone over the United States using the Global Modeling Initiative chemical transport model. We discuss the roles of meteorology, emissions, and transport from the stratosphere in driving the interannual variability in different regions and seasons. We demonstrate that a hindcast simulation for 1991–2010 can reproduce much of the observed variability and the trends in summertime ozone, with correlation coefficients for seasonally and regionally averaged median ozone ranging from 0.46 to 0.89. Reproducing the interannual variability in winter and spring in the western United States may require higher-resolution models to adequately represent stratosphere-troposphere exchange. Hindcast simulations with fixed versus variable emissions show that changes in anthropogenic emissions drive the observed negative trends in monthly median ozone concentrations in the eastern United States during summer, as well as the observed reduction in the amplitude of the seasonal cycle. The simulation underestimates positive trends in the western United States during spring, but excluding the first 4 years of data removes many of the statistically significant trends in this region. The reduction in the slope of the ozone versus temperature relationship before and after major emission reductions is also well represented by the model. Our results indicate that a global model can reproduce many of the important features of the meteorologically induced ozone variability as well as the emission-driven trends, lending confidence to model projections of future changes in regional surface ozone.

1. Introduction

Ozone is a pollutant with adverse impacts on human health and vegetation [e.g., *Lefohn and Foley*, 1993; *Lippmann*, 1989] and is also an important greenhouse gas in the upper troposphere. In the United States, the Clean Air Act establishes a standard for the 3 year average of the annual fourth highest 8 h maximum daily ozone [Environmental Protection Agency (EPA), 2006]. This standard was set at 0.08 ppm in 1997 and revised to 0.075 ppm in 2008, and a further reduction is being considered.

The maximum daily 8 h average (MDA8) surface ozone at monitoring sites in the U.S. shows a decrease of 7% over 1991–2000 [Environmental Protection Agency (EPA), 2001] as well as a 9% decrease from 2001 to 2010 [Environmental Protection Agency (EPA), 2011]. The NO_x Budget Program led to substantial decreases in NO_x emissions beginning in 1999 [e.g., *Frost et al.*, 2006]. The NO_x State Implementation Plan (SIP) Call, which started in 2003, led to an especially large decrease in eastern U.S. ozone between 2002 and 2004 [EPA, 2011]. Reductions in NO_x emissions between 1999 and 2005 are evident in satellite observations of NO₂ columns over the eastern U.S. [Kim et al., 2006]. Satellite-based emission estimates also show decreases in eastern U.S. NO_x emissions from 2003 to 2006 and from 2006 to 2009 [Lamsal et al., 2011]. Accounting for meteorological variability, ozone during the May through September ozone season in the eastern U.S. decreased by an average of 13% between the pre-SIP and post-SIP Call periods [Gego et al., 2007], with large decreases downwind of the Ohio River Valley [Godowitch et al., 2008]. The decrease is present in both urban and rural sites, with the largest decreases occurring at the high end of the distribution [Butler et al., 2011].

Summertime ozone reductions are seen in polluted locations over the past two decades despite increases in daytime temperature [Bloomer et al., 2010]. Examining rural sites for 1990–2010, Cooper et al. [2012] found significant negative trends throughout the eastern U.S. in summer for the 50th and 95th percentiles and for the 95th percentile in spring.

While peak ozone concentrations have decreased in the eastern U.S. during the ozone season, some sites also show increases in ozone at the low end of the distribution [Lefohn *et al.*, 2010; Cooper *et al.*, 2012] that may be due to reduced titration by NO or to increases in baseline ozone [Lin *et al.*, 2000; Cooper *et al.*, 2012], which is the ozone observed at sites without the presence of recent local pollution influence [Dentener *et al.*, 2010]. A modeling study by Fiore *et al.* [2002] found increases in ozone between 1980 and 1995 at the lower half of the distribution due to increases in Asian emissions. Observations also show increasing ozone at some eastern sites in winter and early spring [Bloomer *et al.*, 2010; Cooper *et al.*, 2012], especially at the low end of the ozone distribution [Simon *et al.*, 2015].

In contrast to the negative trends in the eastern U.S., Jaffe and Ray [2007] found positive trends in surface ozone in all seasons at rural and remote sites in the western United States for 1987–2004. An east-west contrast in U.S. surface ozone trends is thus present in spring and summer [Cooper *et al.*, 2012]. Jaffe and Ray [2007] suggest that changes either in regional emissions, biomass burning, or Asian emissions could be responsible for the western trends. Observations in the free troposphere also show a positive trend in springtime ozone over western North America, with measurements impacted by transport from Asia showing the largest increase [Cooper *et al.*, 2010]. Ozonesondes from Boulder, CO, and Edmonton, Alberta, show a decrease in free tropospheric ozone between the late 1980s and the mid-1990s, followed by a small increase [Oltmans *et al.*, 2013].

Numerous studies have investigated changes in baseline ozone over the United States [Vingarzan, 2004, and reference therein]. Increases in baseline ozone concentrations from the 1980s to early 2000s observed in inflow to the U.S. West Coast [Jaffe *et al.*, 2003] and over the North Pacific [Parrish *et al.*, 2004] were attributed to rising emissions of ozone precursors from Asia. Chan and Vet [2010] found mostly negative trends in baseline ozone from 1997 to 2006 for the eastern U.S. and Canadian sites but no significant trend in California. Parrish *et al.* [2009] report a springtime trend for the North American west coast marine boundary layer of 0.46 ± 0.13 ppbv yr⁻¹, as well as significant trends in summer and winter. Parrish *et al.* [2012] find a 1% yr⁻¹ increase in baseline ozone prior to the year 2000 in the northern midlatitudes considering sites in North America, Europe, and Asia.

Pozzoli *et al.* [2011] conducted a global model simulation for 1980–2005. They found that anthropogenic emissions and natural variability had competing effects on surface ozone over much of the U.S., but their simulation did not reproduce the observed negative ozone trends in the eastern U.S. in summer. Koumoutsaris and Bey [2012] found that a global model simulation for 1991–2005 could reproduce negative trends in summertime ozone over the eastern U.S. but underestimated positive trends in the western U.S. They suggest that the underestimation of the western trends could be due to an underestimation of Asian emission trends or trans-Pacific transport or to changes in stratosphere-troposphere exchange (STE). We examine these potential causes of the underestimation of western trends and extend the analysis of trends and variability to all four seasons.

Predicting future changes in surface ozone concentrations requires models to accurately represent the response of ozone to changes in emissions and meteorology. This study quantifies the ability of a global chemical transport model (CTM) hindcast to represent this response for 1991–2010. We investigate the roles of stratosphere-troposphere exchange, changes in emissions, and meteorological variability in driving the ozone trends and year-to-year variations in different seasons and regions of the United States.

2. Methods

2.1. Observations

Environmental Protection Agency (EPA)'s Clean Air Status and Trends Network (CASTNET) monitors air quality in rural areas throughout the United States. We use CASTNET hourly ozone data from 1991 to 2010 from sites that have data coverage for 1990–2010. We also use ozone data from the National Park Service and the University of Albany's Whiteface Mountain Summit site for a total of 53 stations. The stations and their locations are listed in Table S1 in the supporting information. Following Cooper *et al.* [2012], we use only daytime data (11:00–16:00 local time), since the boundary layer is well mixed at this time. Focusing on daytime data avoids model-data mismatches due to errors in model representation of the nighttime boundary layer. The hourly data from all days within a given month are pooled together for the calculation of the mean and percentiles for the month. If more than half the hourly data for a given month and site is missing, that month is excluded from the analysis of the site.

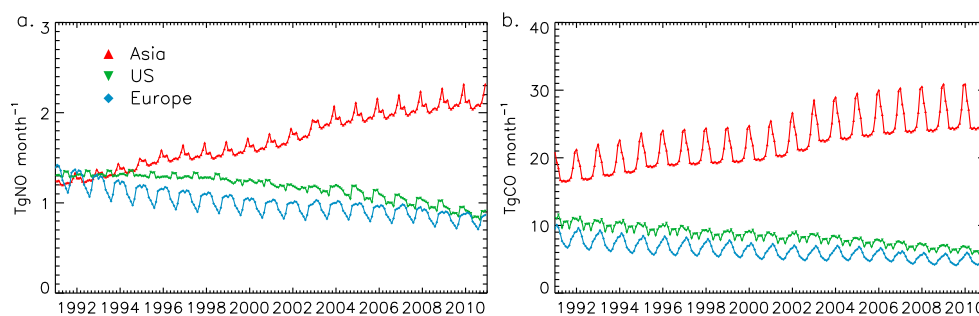


Figure 1. Anthropogenic emissions of (a) NO and (b) CO for each month of our study period are shown for Asia (red), USA (green), and Europe (blue).

Satellite observations of NO₂ provide a valuable constraint on NO_x, an important driver of ozone trends. The Ozone Monitoring Instrument (OMI) [Levelt *et al.*, 2006] on the NASA Aura satellite [Schoeberl *et al.*, 2006] provides tropospheric NO₂ columns beginning in mid-2004. We use the OMI NO₂ product [Bucsela *et al.*, 2013; Lamsal *et al.*, 2014], available at http://disc.sci.gsfc.nasa.gov/Aura/data-holdings/OMI/omno2_v003.shtml, to evaluate our simulated NO₂ columns.

2.2. Model Simulations

This study uses the Global Modeling Initiative (GMI) chemical transport model (CTM) driven by meteorology from the Modern-Era Retrospective Analysis for Research and Applications (MERRA) [Rienecker *et al.*, 2011]. The MERRA fields are regridded from the original $0.667^{\circ} \times 0.5^{\circ}$ resolution to the resolution of the CTM. The GMI CTM includes tropospheric and stratospheric chemistry with 124 species and over 400 reactions [Duncan *et al.*, 2007; Strahan *et al.*, 2007]. The simulations used in this study have $2^{\circ} \times 2.5^{\circ}$ horizontal resolution. GMI uses the 72 vertical levels of MERRA, which extend from the surface to 0.01 hPa. We sample the model hourly at the locations of the surface observations and use only the daytime (11:00–16:00 local time) hours for a self-consistent comparison with the observation data set. We typically sample the model at the surface level. However, the data set includes several sites at elevations substantially above the modeled terrain, and in some of these cases we sample at the model level best corresponding to the altitude of the observation. Table S1 shows the model level sampled for each site. In addition, we average the model output between 01:00 and 02:00 P.M. local time for consistency with the timing of the Aura overpass for comparison with OMI observations.

Our standard simulation (Std) for 1990–2010 includes monthly and interannually varying emissions of CO, NO, and nonmethane hydrocarbons. Anthropogenic emissions are based on the Emissions Database for Global Atmospheric Research (EDGAR) 3.2 inventory [Olivier *et al.*, 2005], overwritten with the Criteria Air Contaminant (CAC) inventory (<https://www.ec.gc.ca>) over Canada, the Big Bend Regional Aerosol and Visibility Observational study inventory over Mexico [Kuhns *et al.*, 2005], the European Monitoring and Evaluation Programme (EMEP, <http://www.emep.int>) over Europe, and the Intercontinental Chemical Transport Experiment-B inventory over Asia [Zhang *et al.*, 2009]. Anthropogenic emissions over the United States come from the EPA National Emissions Inventory 2005 inventory (<http://www.epa.gov/ttnchie1/net/2005inventory.html>), with seasonality from the Visibility Improvement State and Tribal Association of the Southeast beginning in 1999. We apply annual scaling factors from the GEOS-Chem model [van Donkelaar *et al.*, 2008], including factors based on the Regional Emission inventory in ASia (REAS) inventory [Ohara *et al.*, 2007] over Asia, to scale the anthropogenic emissions for each year for 1990–2006. The NO_x scaling factors vary geographically within the U.S. and thus account for regional differences in NO_x reductions. For 2007–2010, we apply annual-scale factors to the U.S. and European emissions on a country-wide basis using the national emission totals from EPA (<http://www.epa.gov/ttn/chie1/trends/index.html>) and EMEP (http://www.ceip.at/ms/ceip_home1/ceip_home/webdab_emepdatabase/reported_emissiondata/), respectively. We also use the REAS inventory projections for annual scaling of the Asian anthropogenic emissions for 2007–2009 and then repeat 2009 emissions in 2010. Anthropogenic emissions from the U.S. and Europe show a decrease with time, while Asian anthropogenic emissions increase (Figure 1). The decrease in U.S. NO_x emissions is particularly strong during summer.

Biomass burning emissions for 1997–2010 come from the Global Fire Emissions Database version 3 (GFED3) inventory [van der Werf *et al.*, 2010] and exhibit large year-to-year variability. We derive biomass burning emissions for years prior to 1997 by applying regional-scale interannual variability (IAV) from Duncan *et al.* [2003] to an emission climatology based on the GFED3 data averaged over 2001 to 2009.

Biogenic emissions of isoprene are calculated within GMI using the Model of Emissions of Gases and Aerosols from Nature (MEGAN) model [Guenther *et al.*, 1999, 2000] and are dependent on temperature, photosynthetically active radiation, and climatological leaf area index. Soil emissions of NO_x are also calculated online with temperature and precipitation dependencies, based on Yienger and Levy [1995]. Consequently, isoprene and soil NO_x emissions vary from year to year. Interannually varying lightning NO_x emissions are calculated online following Allen *et al.* [2010]. Aircraft NO_x emissions are the same each year. Methane concentrations are specified as a lower boundary condition based on observations and include a latitude dependence. The global mean-specified methane concentration increases by 9% between January 1991 and January 2010.

We conduct an additional simulation for 1990–2010, called EmFix, using anthropogenic and biomass burning emissions fixed at year 2000 levels. Comparison of the EmFix simulation with the standard simulation allows us to separate the contribution of changing emissions from other sources of variability. Although soil and lightning NO_x as well as isoprene vary year to year, the emissions in the EmFix simulation are the same as those in the standard simulation since the meteorology is the same in both simulations. The specification of methane concentrations is the same as in the standard simulation.

We conduct a sensitivity study for 2003–2010, called USIAV, that has the same time-dependent anthropogenic emissions as the standard simulation over the United States but constant emissions as in EmFix everywhere else. Comparison of USIAV with EmFix and the standard simulation allows us to isolate the impact of changes in U.S. emissions from that of changing emissions elsewhere.

Two additional sensitivity simulations are discussed in section 3. One is a high-resolution simulation with the same inputs as the standard simulation but runs at 1° × 1.25° resolution. The other, further described in section 3.2.3, uses an alternate NO_x emission scenario for 2006–2010 based on scaling factors from OMI.

Stratospheric ozone can make important contributions to surface ozone concentrations, particularly at high-altitude sites in the western U.S. [Lin *et al.*, 2012]. Koumoutsaris and Bey [2012] recommended that future global hindcasts use models with a fully coupled stratosphere and troposphere. The GMI CTM has a full treatment of stratospheric chemistry and realistic transport in the lowermost stratosphere [Strahan *et al.*, 2007, 2013]. Here we analyze the impact of stratospheric ozone on variability and trends in surface ozone over the U.S. using a stratospheric ozone tracer, O3Strat. Several methods of defining the stratospheric ozone contribution are found in the literature, and the choice of definition influences the inferred contribution [Hess and Lamarque, 2007; Zhang *et al.*, 2014]. O3Strat in our study is set equal to the ozone concentration above the tropopause. Below the tropopause, O3Strat has no source and undergoes loss based on interannually varying monthly mean loss rates archived from a simulation with interactive chemistry. The tropopause is defined following the approach of Prather *et al.* [2011] using an artificial tracer, e90, where its value is 85 ppb.

Section 3.4 compares results from the GMI CTM to results from the GEOS-5 Chemistry-Climate Model (GEOSCCM) [Oman *et al.*, 2011]. The GEOSCCM uses the same chemical mechanism as GMI. We use the GEOSCCM's Ref-C1 simulation from the Chemistry-Climate Model Intercomparison project [Eyring *et al.*, 2013], which is driven by observed sea surface temperatures and uses time-dependent anthropogenic and biomass burning emissions. While these emissions differ from those of our standard simulation, the GEOSCCM simulation also has a positive emission trend in Asia and negative trends over the United States and Europe. This GEOSCCM simulation uses 2 × 2.5° resolution, consistent with our standard GMI hindcast.

2.3. Trend Estimation

We calculate the modeled and observed temporal trends at each site for each month for the mean, median, 5th percentile, and 95th percentile of the daytime ozone distribution. The percentile and mean values for each month and year are calculated from all hourly daytime values (11:00–16:00 local time) for that month and year. Observations falling within a single grid box are then averaged together. We use linear regression to determine the trend for 1991–2010 for each month. The trend is considered statistically significant if it differs from zero by more than 2 times the standard error on the trend. We also calculate the correlation

Table 1. Regional Comparison of Simulations With Observations: Temporal Correlation, Bias, and Standard Deviation of Regionally Averaged Ozone

Percentile	Season	Region					
		New England ^a	Mid-Atlantic ^b	Southeast ^c	Midwest ^d	Mountain West ^e	California ^f
Correlation Coefficient ^g : <i>r</i> (Std Simulation, Obs), <i>r</i> (EmFix Simulation, Obs)							
5th	Jan/Feb	0.55, 0.50	0.75, 0.67	0.75, 0.71	0.52, .39	0.47, 0.45	0.53, 0.54
	Mar/Apr	0.38, 0.38	0.47, 0.48	0.46, 0.57	0.17, 0.17	0.23, 0.12	0.58, 0.55
	Jul/Aug	0.45, 0.29	0.68, 0.53	0.85, 0.87	0.89, 0.82	0.73, 0.66	0.32, 0.18
	Oct/Nov	0.40, 0.43	0.70, 0.63	0.62, 0.64	0.83, 0.81	0.48, 0.45	0.40, 0.37
50th	Jan/Feb	0.79, 0.80	0.68, 0.69	0.74, 0.82	0.64, 0.64	0.49, 0.33	0.28, 0.16
	Mar/Apr	0.36, 0.37	0.41, 0.44	0.59, 0.65	0.20, 0.22	0.58, 0.37	0.22, 0.07
	Jul/Aug	0.53, .27	0.79, 0.71	0.89, 0.87	0.86, 0.75	0.77, 0.65	0.46, 0.22
	Oct/Nov	0.26, 0.42	0.81, 0.76	0.77, 0.76	0.67, 0.63	0.70, 0.60	0.58, 0.53
95th	Jan/Feb	0.71, 0.65	0.66, 0.72	0.90, 0.90	0.29, 0.33	0.46, 0.29	0.25, 0.20
	Mar/Apr	0.20, 0.20	0.73, 0.76	0.71, 0.61	0.58, 0.64	0.76, 0.57	0.30, 0.24
	Jul/Aug	0.77, 0.67	0.85, 0.72	0.86, 0.79	0.82, 0.74	0.69, 0.50	0.45, 0.14
	Oct/Nov	0.76, 0.76	0.46, 0.46	0.85, 0.88	0.63, 0.38	0.48, 0.25	0.43, 0.32
Mean Bias (ppbv); Mean Percent Bias (%) ^h in Parentheses							
5th	Jan/Feb	-0.13 (-1)	0.49 (4)	3.9 (24)	-0.92 (-8)	-4.4 (-12)	6.1 (22)
	Mar/Apr	6.2 (20)	5.9 (23)	7.9 (28)	4.4 (17)	-2.1 (-5)	1.8 (5)
	Jul/Aug	11 (50)	16 (51)	21 (67)	9.7 (31)	4.6 (11)	-6.9 (-17)
	Oct/Nov	9.3 (61)	5.2 (35)	7.8 (40)	3.7 (30)	0.84 (3)	6.2 (21)
50th	Jan/Feb	-0.13 (0)	-3.4 (-11)	-3.7 (-11)	-3.6 (-13)	-3.5 (-8)	8.3 (8)
	Mar/Apr	0.19 (0)	-3.2 (-7)	-2.4 (-5)	-4.9 (-11)	4.3 (-8)	-0.75 (-2)
	Jul/Aug	13 (33)	13 (24)	12 (23)	6.3 (12)	2.9 (5)	-13 (-21)
	Oct/Nov	4.9 (16)	-0.43 (-1)	1.2 (3)	-2.3 (-8)	-1.3 (-3)	1.1 (3)
95th	Jan/Feb	-2.1 (-5)	-5.3 (-13)	-6.6 (-13)	-5.1 (-13)	-3.8 (-7)	1.8 (4)
	Mar/Apr	-3.3 (-6)	-9.5 (-15)	-8.7 (-13)	-12 (-20)	-6.1 (-10)	-5.2 (-10)
	Jul/Aug	6.4 (10)	1.6 (2)	0.42 (1)	-4.4 (-6)	-1.4 (-2)	-19 (-24)
	Oct/Nov	2.9 (7)	-3.0 (-6)	-2.2 (-4)	-7.4 (-14)	-1.1 (-2)	-5.2 (-9)
Standard Deviation (ppbv): Standard Deviation (Obs); Standard Deviation (Std Simulation)							
5th	Jan/Feb	3.6; 2.2	3.5; 2.1	3.8; 2.7	3.0; 2.1	2.4; 2.4	2.7; 2.2
	Mar/Apr	3.0; 1.8	2.7; 2.2	3.4; 1.7	3.0; 2.2	1.8; 1.3	2.6; 2.6
	Jul/Aug	1.6; 2.7	3.5; 3.2	5.3; 4.8	3.8; 3.9	3.2; 3.2	3.3; 3.3
	Oct/Nov	2.0; 1.1	3.2; 2.3	3.8; 2.2	3.1; 2.5	1.8; 1.6	3.1; 2.5
50th	Jan/Feb	1.8; 1.6	1.9; 1.7	1.7; 1.9	2.0; 2.5	1.8; 1.4	1.9; 1.3
	Mar/Apr	2.1; 0.92	1.5; 1.5	2.1; 1.5	1.3; 1.6	1.9; 1.2	2.6; 1.2
	Jul/Aug	2.4; 3.1	5.6; 3.9	6.3; 5.3	5.2; 4.0	3.3; 2.2	3.5; 3.1
	Oct/Nov	1.5; .92	2.4; 1.8	4.2; 2.8	2.4; 2.4	1.8; 1.7	3.5; 1.7
95th	Jan/Feb	1.9; 1.5	1.8; 1.6	2.3; 2.4	2.2; 1.7	2.1; 1.4	2.7; 1.8
	Mar/Apr	3.4; 2.2	3.2; 2.4	2.8; 2.3	2.7; 2.7	2.7; 1.7	2.7; 2.0
	Jul/Aug	7.0; 4.1	9.8; 5.1	8.6; 6.9	8.7; 5.1	4.0; 2.1	4.8; 4.1
	Oct/Nov	3.3; 3.1	4.6; 4.1	6.1; 4.8	5.9; 4.1	1.9; 1.9	5.5; 2.4

^aNew England includes the following sites: APTR-MG, SARA-ST, CACO-XX, WFMS, WST109, ASH135.
^bMid-Atlantic includes VPI120, CDR119, PED108, SHN418, PAR107, LRL117, BEL116, ARE128, PSU106, MKG113, KEF112, WSP144, CTH110.
^cSoutheast includes CVL151, SND152, GAS153, ESP127, SPD111, GRSM-LR, COW137, BLRI-RO, GRSM-CM, PNF126.
^dMidwest includes ALH157, BVL130, VIN140, SAL133, OXF122, DCP114, LYK123, ANA115, UVL124.
^eMountain West includes Yell-Merge, PND165, CNT169, GTH161, ROMO-LP.
^fCalifornia includes LAVO-ML, PINN-ES, SEKI-LK.
^gDetrended correlations; the bold text indicates that the correlation is significant at the 95% level.
^hMean percent bias = mean(Std simulation/obs - 1) × 100.

between the modeled and observed IAVs for each month after detrending both the model and observations. We detrend the time series by removing the linear fit to the monthly data.

3. Results and Discussion

3.1. Interannual Variability

3.1.1. Model Representation of Regional Ozone Concentrations and Variability

We examine the ability of the hindcast to reproduce the concentrations and year-to-year variability seen in the CASTNET data for each season for six regions: California, the Mountain West, Midwest, Southeast, mid-Atlantic,

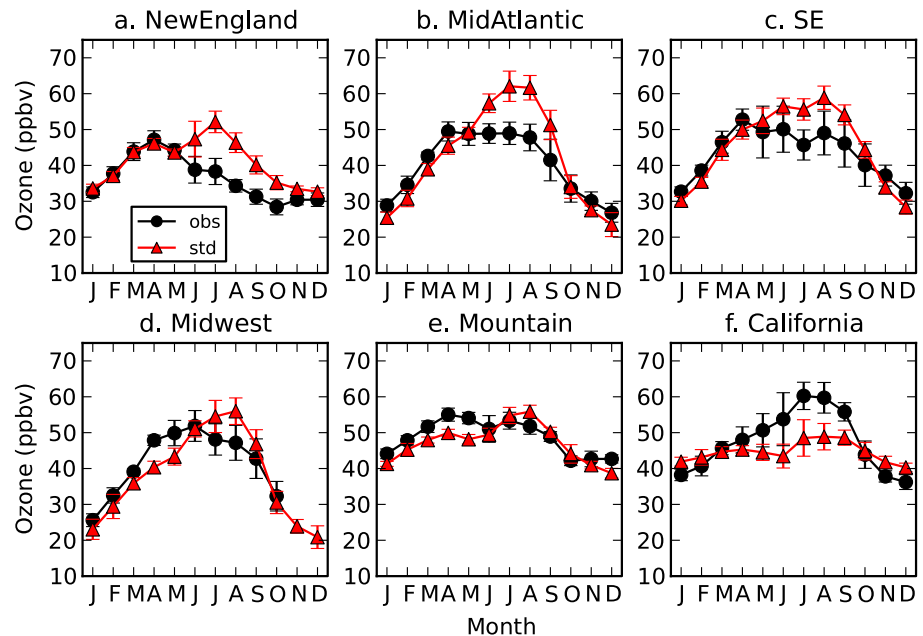


Figure 2. Seasonal cycle in median daytime (11:00–16:00 local time) ozone for observations (black) and the standard simulation (red) averaged over 2005 to 2010 for the six regions defined in Table 1: (a) New England, (b) mid-Atlantic, (c) Southeast, (d) Midwest, (e) Mountain West, and (f) California. Error bars represent the standard deviation across all years.

and New England. The stations included in each region are shown in Figure S1 in the supporting information and listed in Table S2 and the footnote of Table 1. We average over the region's sites before calculating statistics for each region. We also average together 2 months for each season for the analysis of regional means. Using 2 rather than 3 months per season allows us to exclude May from the spring average, as May ozone trends often show more similarity to those in summer than spring.

We note that nearby sites typically show similar IAV, as shown by the correlation coefficients between example sites from four regions shown for July in Figure S2. Strong correlation between nearby sites is evident in the Midwest and Southeast, while weaker correlations are seen for some sites in New England such as the high-altitude Mount Greylock Summit site. Sites in the Mountain West are located farther apart from one another, but strong correlations between sites are present, as also found by *Jaffe* [2011].

The simulated median ozone is biased high compared to observations in summer and slightly low in winter and spring for most regions (Figure 2 and Table 1), with the peak ozone concentration occurring later in the year in the standard simulation than in the observations. Large high biases in mean summer ozone were also present in the eastern U.S. in most of the models that participated in the Hemispheric Transport of Air Pollution intercomparison [*Fiore et al.*, 2009], and the smaller low bias in other seasons in the Mountain West is also seen in the multimodel mean in that study. Possible causes of the low bias (a few parts per billion) in the Mountain West include insufficient transport from Asia or the stratosphere, as well as difficulty resolving flow over complex terrain. The simulation underestimates the amplitude of the observed seasonal cycle for California, but we note that a single site, Sequoia/Kings Canyon, drives the large amplitude in the observations. Excluding this site reduces but does not eliminate the underestimate. High bias in the eastern regions and low bias in California in summer is consistent with the biases seen in other model studies [*Emery et al.*, 2012; *Tong and Mauzerall*, 2006].

For the lowest 5th percentile ozone values, the model is biased high in most seasons and regions (Table 1). In contrast, the model is generally biased low for the 95th percentile except in the eastern regions in summer, indicating that it does not capture the magnitude of the most extreme events. The high bias at low percentiles is consistent with previous studies using regional [*Hogrefe et al.*, 2011] and global models [*Emery et al.*, 2012; *Fiore et al.*, 2002]. The model underestimates the standard deviation of the observations for most regions and seasons but reproduces the observed feature of greater variability in summer compared to other seasons for most regions and percentiles (Table 1).

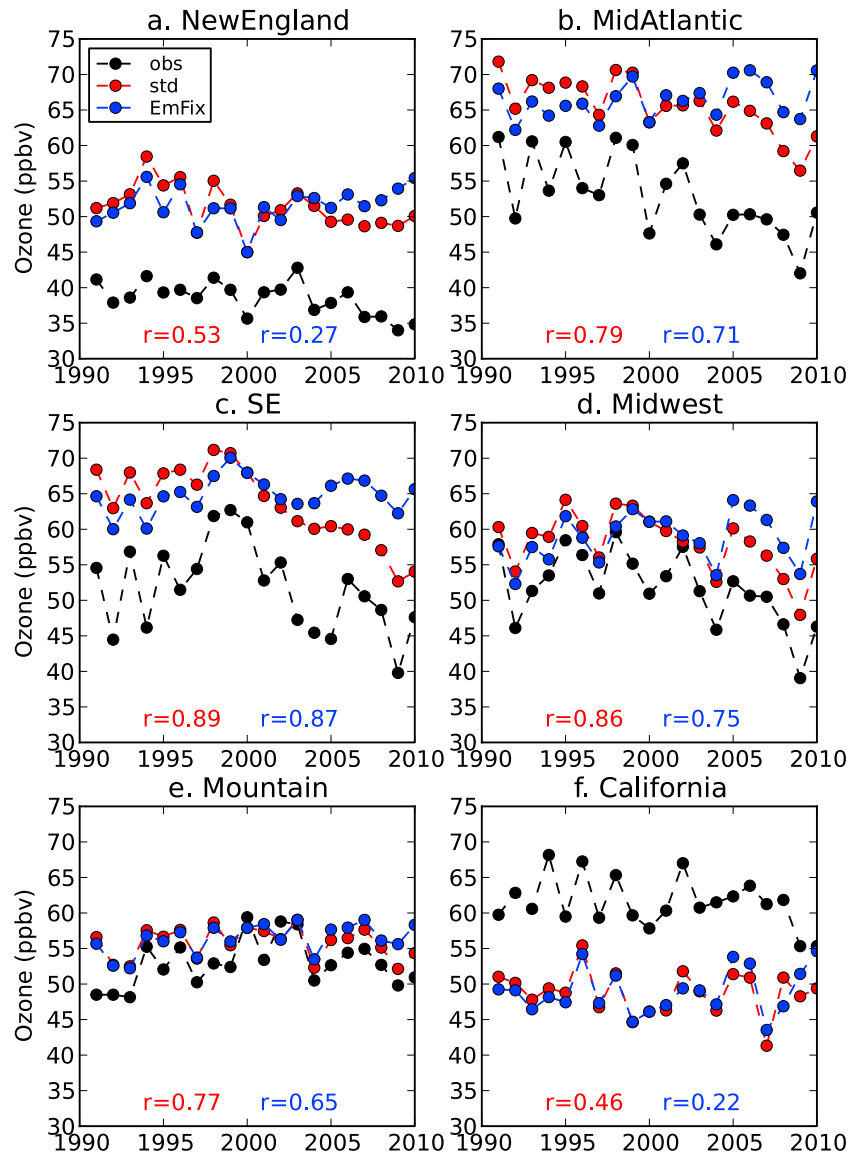


Figure 3. Interannual variability in median ozone averaged for July and August for six regions: (a) New England, (b) mid-Atlantic, (c) Southeast, (d) Midwest, (e) Mountain West, and (f) California. Median ozone values from multiple sites within each region are averaged together to create the regional means. We compare the standard simulation (red) and EmFix simulation (blue) to the observed values (black). The correlation coefficient (r) between the simulated and observed IAIVs in the detrended 2 month averages is shown for each region for the standard (red) and EmFix (blue) simulations. The time series are plotted without detrending.

Figure 3 shows the median ozone time series for July/August for the six regions. While the variability is similar in both the standard and EmFix simulations, the observed decrease in ozone in the Midwest, Southeast, mid-Atlantic, and New England beginning in the early 2000s is evident only in the standard simulation (Figure 3). Anthropogenic NO_x emissions in these regions decreased by about 30% between 2000 and 2010 in the standard simulation, driving the decrease in ozone. Similar percent decreases in anthropogenic NO_x occurred in the Mountain West and California, but the absolute changes in those regions are smaller, and the impact on ozone is less pronounced.

The simulations show strong correlations with the CASTNET observations ($r > 0.7$) in the Mountain West, Midwest, mid-Atlantic, and Southeast but have weaker correlations for California and New England (Table 1 and Figure 3). Statistically significant correlations are present in the mid-Atlantic and Southeast regions in almost all seasons and percentiles (Table 1). The standard and EmFix simulations show similar correlations with

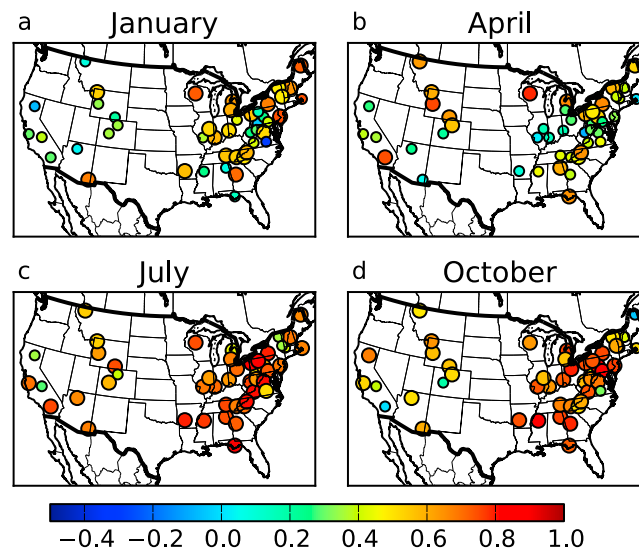


Figure 4. The correlation coefficient (r) of the simulated IAV with the observed interannual variability in detrended monthly median daytime ozone at each site for (a) January, (b) April, (c) July, and (d) October. The larger circles indicate that the correlations are statistically significant.

the data after detrending, indicating that meteorology drives most of the IAV once any long-term trend is removed. An exception to this is New England in summer, where the observations show a strong decrease at the end of the time series not captured by the EmFix simulation (Table 1 and Figure 3). The model grid boxes covering some of the New England sites contain a mix of land and ocean. Complex terrain may be a factor in the weaker model performance in California. In addition, both California and New England show substantial variability between sites, as noted above.

Both the observations and model simulations show a strong dip in summertime ozone in 2009 in several regions (Figure 3). This feature is particularly prominent in the Midwest. July–August of 2009 was exceptionally cool in the Midwest, and four Midwestern states plus Virginia and Pennsylvania reached record cool July temperatures [Arndt *et al.*, 2010]. The EmFix simulation demonstrates the impact of this anomalously cool summer on ozone concentrations. Simulated ozone concentrations, ozone production, and soil NO_x emissions all decrease in this region from 2008 to 2009.

We also examine the correlation between the observed and simulated IAVs in detrended monthly median daytime ozone at each individual site and month. The Pearson's correlation coefficients are shown in Figure 4 for January, April, July, and October. In January, the model shows significant correlations with the observed IAV at some but not all eastern sites, while the correlation at most western sites is much weaker. More statistically significant correlations are seen in the west in April, but there are weak correlations in Illinois and the Ohio River Valley. In July and October (Figures 4c and 4d), significant strong correlations are present at almost all eastern sites and many of the western sites. Overall, both the standard simulation and the EmFix simulation (not shown) have strong correlations with the observed IAV for summer and autumn months but have greater difficulty reproducing the winter and spring IAVs. This is consistent with the findings of Pozzoli *et al.* [2011], who report stronger correlations at U.S. sites for summer versus winter. We discuss drivers of ozone IAV in different seasons in the following sections.

3.1.2. Impact of Meteorology on IAV in Summer and Winter

We examine the meteorological factors that allow the model to capture the summertime IAV seen in Figures 3 and 4. Surface ozone observations show increases with temperature and decreases with relative humidity, with temperature of greater importance in the northeastern U.S. and humidity important further south [Camalier *et al.*, 2007]. Temperature and mixing height are important drivers of ozone variability at urban sites in the southwestern United States [Wise and Comrie, 2005]. Episodes of high ozone are typically associated with stagnant conditions, clear skies, and high-pressure systems [Hegarty *et al.*, 2007; Logan, 1989; Seaman and Michelson, 2000]. Consequently, the link between temperature and stagnation contributes to the correlation between temperature and ozone concentration [Jacob *et al.*, 1993]. The frequency of midlatitude cyclones is

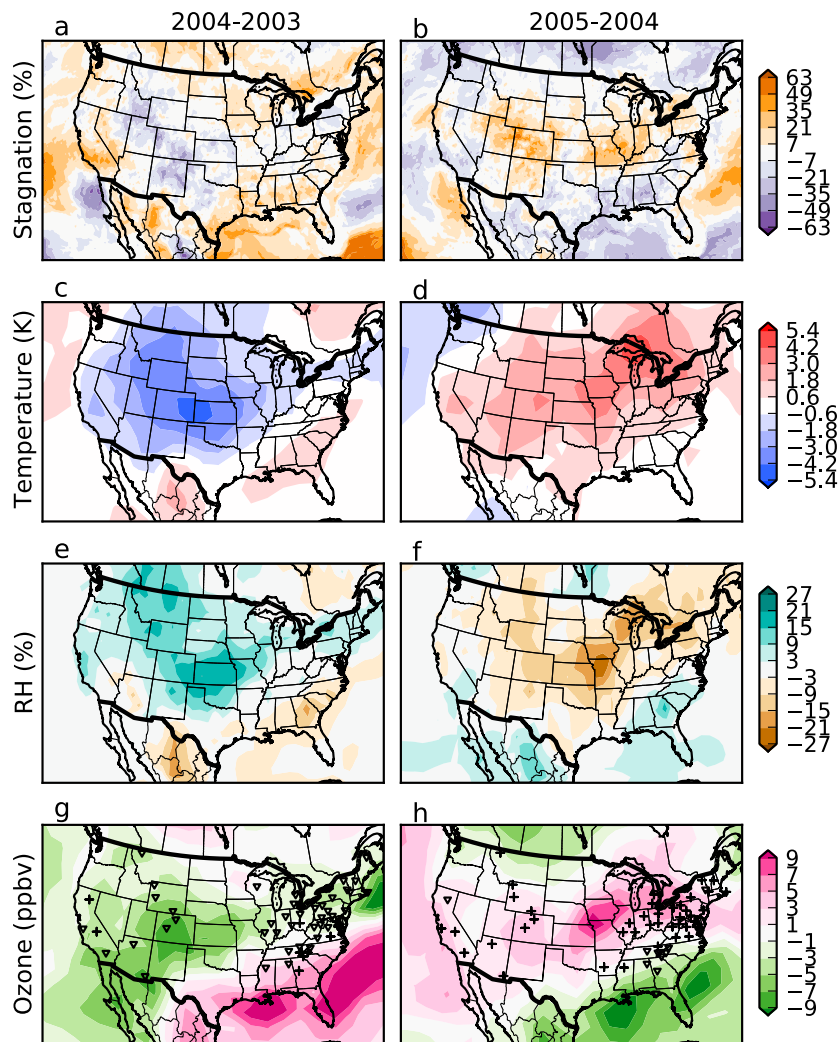


Figure 5. July differences in (a and b) Air Stagnation Index (% stagnation days), (c and d) MERRA surface temperature (K), (e and f) MERRA relative humidity (%), and (g and h) monthly mean simulated ozone (ppbv) for (left column) 2004–2003 difference and (right column) 2005–2004 difference. The sign of the observed change in daytime ozone is indicated by cross symbols for positive changes and triangles for negative changes.

anticorrelated with high ozone and stagnant conditions, since the cyclone passage clears out the polluted air mass [Leibensperger et al., 2008]. The temperature dependence of peroxyacetylnitrate lifetime and isoprene emissions may also contribute to the ozone versus temperature relationship [Sillman and Samson, 1995].

Figure 5 compares the Air Stagnation Index [Wang and Angell, 1999], surface temperature and relative humidity from MERRA, and our simulated surface ozone concentrations for the month of July in 2003, 2004, and 2005. These years were selected because they show ozone differences in several different regions of the country. The Air Stagnation Index, downloaded from <ftp://ftp.ncdc.noaa.gov/pub/data/cmb/societal-impacts/air-stagnation/data/>, identifies a stagnation day when there is no precipitation, the wind speed at 500 mb is less than 13 m s^{-1} , and the sea level geostrophic wind is less than 8 m s^{-1} or 8.8 m s^{-1} if there is also a temperature inversion below 850 mb. The wind and temperature data for the stagnation index are from the National Centers for Environmental Prediction/National Center for Atmospheric Research reanalysis [Kalnay et al., 1996]. The lower ozone in the Midwest and Southwest in 2004 compared to 2003 corresponds to lower temperatures, higher relative humidity (RH), and fewer stagnation days in that region. The elevated ozone seen in Missouri and Iowa in 2005 compared to 2004 corresponds to more stagnation days, higher temperatures, and lower RH in that region. Simulated soil NO_x emissions are enhanced in this region in 2005 compared to 2004. Higher ozone production rates in 2005 are present throughout the northeastern

U.S. In contrast, lower ozone is present in the Southeast in 2005, where there is higher RH and fewer stagnation days than in 2004. Ozone production rates and isoprene emissions are higher in the Southeast in 2004 than in 2003 or 2005. The spatial distribution of the observed daytime ozone differences shows general agreement with the simulated differences in monthly mean ozone (Figures 5g and 5h).

To understand the simulated IAV in winter and spring, we focus on two regions, New England and the Midwest, with weak springtime correlations with observed IAV. Both regions show strong temporal correlations ($r=0.76$ and $r=0.82$, respectively) between simulated July monthly mean ozone and temperature. The simulated ozone versus temperature correlations drop to $r=0.48$ and $r=0.42$, respectively, in March, and to $r=-0.49$ and $r=-0.20$ in January. The use of realistically varying temperature fields from MERRA helps drive realistic ozone IAV in summer, when photochemical production is highest, but does not lead to strong correlations with observed IAV in winter and spring. The magnitude of the observed variability is also smaller in spring and winter than in summer (Table 1), so the relative importance of model errors is potentially greater. Furthermore, modeling studies show that background ozone, including that from long-range transport or stratosphere-troposphere exchange, makes a larger contribution in spring than summer [Fiore *et al.*, 2003, 2014].

3.1.3. Impact of Stratosphere to Troposphere Transport on IAV in Winter and Spring

A potential source of surface ozone IAV in winter and spring is stratosphere to troposphere transport (STT). STT is expected to make the largest contributions in spring in the western U.S. [Lefohn *et al.*, 2011; Lin *et al.*, 2012; Skerlak *et al.*, 2014; Sprenger and Wernli, 2003; Zhang *et al.*, 2014] and can contribute to summertime ozone as well [Langford *et al.*, 2015; Lefohn *et al.*, 2011]. Skerlak *et al.* [2014] found that deep STT of ozone into the planetary boundary layer reaches a maximum in early spring, but enhancements are present over the western U.S. in all seasons. Observations show elevated surface ozone concentrations related to transport from the upper troposphere or lower stratosphere in California [Langford *et al.*, 2012], Colorado [Langford *et al.*, 2009], and the Pacific Northwest [Ambrose *et al.*, 2011]. There is also year-to-year variability in the influence of STT on surface ozone concentrations [Lefohn *et al.*, 2012]. Lin *et al.* [2015] found an increase in stratospheric ozone reaching the surface in the western U.S. in springs following La Niña.

We use the O3Strat tracer to examine the role of STT in the IAV of surface ozone. The concentration of winter and spring O3Strat at the surface in both the eastern and western U.S. peaks in 1999 in the model. This is consistent with the chemistry-climate model study of Zeng and Pyle [2005], which found enhanced STE in a chemistry-climate model following the 1997–1998 El Niño, as well as the Lin *et al.*'s [2015] study, which found peaks in stratospheric ozone at the surface of the western U.S. in 1999, 2008, and 2011. The simulated 1999 peak is supported by observations that show that 1999 was the year with the greatest number of March and April days with ozone above 65 ppbv at western U.S. sites between 1995 and 2009 [Jaffe, 2011].

Figure 6a shows the temporal correlation for 1991–2010 in mean O3Strat and simulated surface ozone in the EmFix simulation for February, the month when the simulation shows the largest values of O3Strat at the surface over the U.S. Similar results were found for the standard simulation (not shown). Significant correlations are seen across much of the western U.S., with particularly high values in the Northwest. Figure 6b shows the time series of February anomalies for the Glacier National Park site. The mean contribution of O3Strat to simulated surface ozone at the surface at Glacier is 22%. O3Strat is highly correlated with the simulation's surface ozone at Glacier ($r=0.83$), and the similar amplitude of the O3Strat and surface O₃ anomalies indicates that IAV in the stratospheric ozone reaching the surface is an important driver of the simulation's IAV in total ozone. Simulated and observed February mean daytime ozone have a significant correlation ($r=0.57$) at Glacier, stronger than that seen at most other western sites.

The simulation does not show strong correlations between O3Strat and surface ozone later in spring, even though Skerlak *et al.* [2014], using a different reanalysis data set, show that the flux of ozone into the planetary boundary layer over the Rocky Mountains is greatest in March through May. Lin *et al.* [2015] found a correlation of 0.43 between their simulated O3Strat and regional median MDA8 ozone in the western U.S. for April–May of 1990–2012. The correlations in our model in the Northwest are weaker in March than February, and in April there are very few statistically significant correlations over the U.S. The simulation's limited ability to capture the stratospheric influence on surface ozone may be due in part to numerical dissipation of plumes in the Eulerian model [Rastigejev *et al.*, 2010] and the $2 \times 2.5^\circ$ model resolution. Recent studies show that higher-resolution simulations better reproduce deep intrusions of stratospheric ozone [Lin *et al.*, 2012], and increasing resolution impacts the calculation of policy-relevant background ozone in the western U.S.

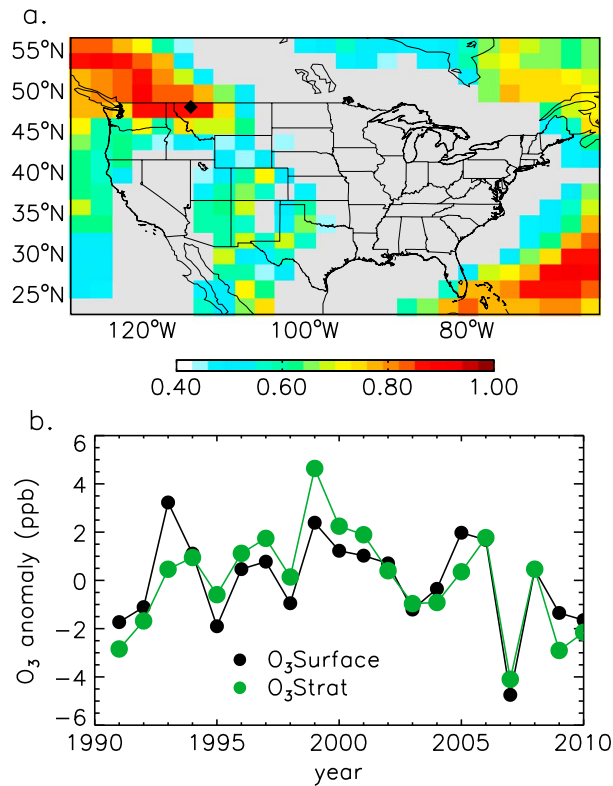


Figure 6. (a) Interannual correlation coefficient (r) between simulated mean February concentrations of surface ozone from the EmFix simulation and the O3Strat tracer at the surface. Grid boxes without a statistically significant correlation are shaded gray. The black diamond indicates the location of the Glacier National Park site. (b) Time series of mean February surface ozone (black) and O3Strat (green) anomalies at the Glacier National Park site.

[Emery et al., 2012; Zhang et al., 2011]. GEOSCCM simulations that use the GMI chemistry mechanism also show that the stratospheric contribution to surface ozone is better reproduced in a simulation at quarter degree resolution than at lower resolutions (E. Nielsen, personal communication, 2014). Consequently, the limited ability of the GMI $2 \times 2.5^\circ$ simulation to capture the IAV in transport of stratospheric ozone to the surface may contribute to the lower correlations in winter and spring, particularly for western sites.

Since processes such as STT are sensitive to model resolution, we repeated our standard hindcast simulation at $1 \times 1.25^\circ$ resolution to determine whether this increase in model resolution improves the simulated IAV. We do not find any substantial improvement in the ozone trends or IAV. However, the higher resolution does reduce the winter and spring biases in California. The impact of increasing resolution is nonlinear, and it is likely that even higher-model resolution is needed to accurately represent smaller-scale transport and chemistry processes. However, Zhang et al. [2014] found that even at $0.5^\circ \times 0.666^\circ$ resolution, their model reproduced the timing but not the magnitude of stratospheric intrusions in the U.S. Intermountain West. Their study used assimilated meteorological fields from GEOS-5.

3.2. Trends

3.2.1. Geographic Distribution of Trends

We quantify the ability of the simulations to reproduce the distribution of observed trends in surface ozone for 1991–2010 and examine the drivers of the observed trends. Figure 7 shows the trends in median ozone from observations, the standard simulation, and the EmFix simulation for 1 month in each season. The negative trends in the eastern U.S. in summer are present in the standard simulation but are absent in the EmFix simulation, confirming the role of emission reductions in reducing summertime ozone in the eastern U.S. This effect is present throughout May–October. The standard simulation also better reproduces the increase in ozone in the western U.S. in January than the EmFix simulation, as it does at some eastern sites, although both simulations underestimate the observed trends. This increase in ozone occurs despite a decrease in the regional anthropogenic NO_x emissions. Observations in the western U.S. show a mixture of positive and negative trends, with positive trends particularly prominent in spring [Cooper et al., 2012], but these trends are generally not well captured by either model simulation (Figure 7). The standard simulation also underestimates the magnitude of the positive trend at some western sites in summer, consistent with the results of Koumoutsaris and Bey [2012]. The causes of the observed trends are discussed later in this section.

We investigate the earlier (1991–2000) and later (2001–2010) portions of the time series separately to identify different trend drivers. Figure 8 shows the July trends for these two periods for the observations (gray), standard simulation (red), and EmFix simulation (blue). The earlier period (Figure 8a) shows mostly increases in the observations west of 80°W , switching to decreases further east (and north). In contrast, the later decade (Figure 8b) shows negative trends in the observations across most of the U.S. The shift toward negative trends is better captured in the standard simulation, with the emissions playing a dominant role.

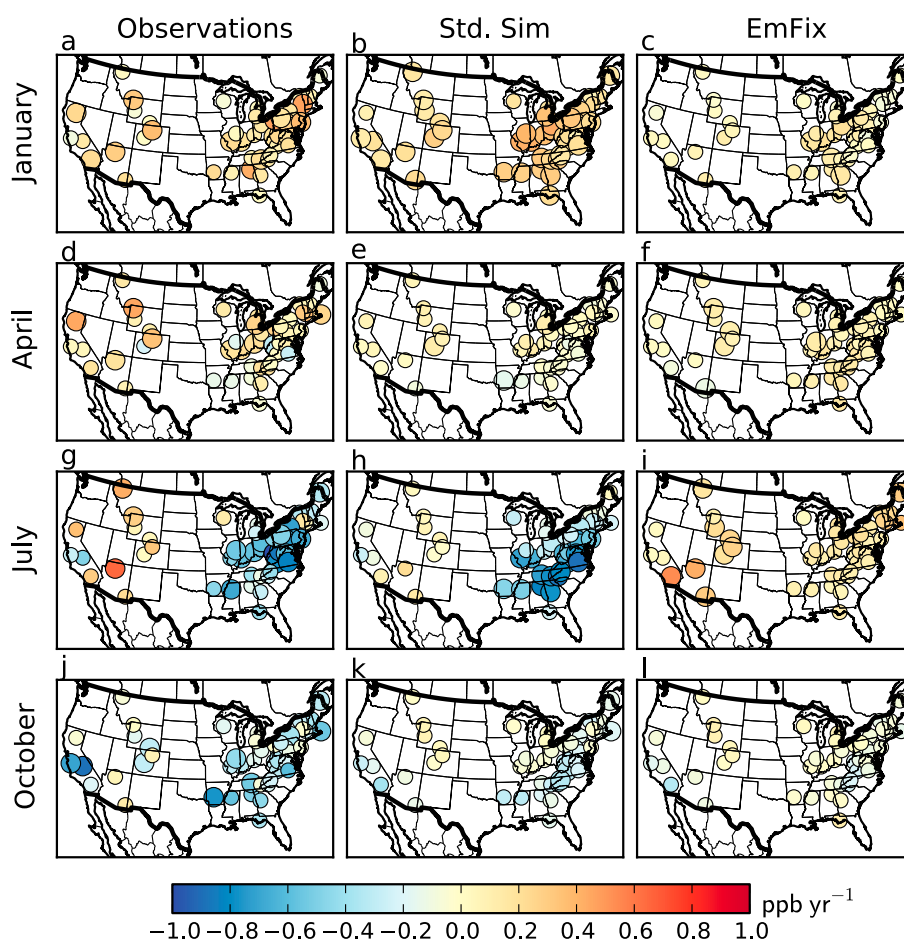


Figure 7. Trends in monthly median daytime ozone for 1991–2010 in (left column) surface observations, (middle column) standard simulation, and (right column) EmFix simulation for (a–c) January, (d–f) April, (g–i) July, and (j–l) October. The larger circles indicate that the trend is statistically significant.

Since changes in NO_x are a major driver of ozone changes, we compare the tropospheric NO_2 column from our standard simulation to observations from OMI [Bucsela et al., 2013; Lamsal et al., 2014]. Figure 9 shows NO_2 over the U.S. for 2005 and 2010, as well as the 2005–2010 differences, for OMI and the standard simulation sampled at the OMI overpass time. The simulation captures many features of the observed distribution, including the high concentrations extending east from the Ohio Valley, the lower concentrations in the western U.S., and enhanced concentrations over Los Angeles and other West Coast cities. The simulation overestimates NO_2 over Los Angeles and San Francisco in both 2005 and 2010, possibly contributing to the low correlation between the simulation and observations in California (Table 1), and the region of highest emissions is centered slightly too far south in 2005 (Figure 9). The simulation reproduces both the magnitude and distribution of the 2005 versus 2010 difference in OMI NO_2 well, although it does not capture all of the small changes seen by OMI in the western U.S. The simulation underestimates the observed decrease in NO_2 over southern New England, consistent with the underestimate of the 2001–2010 ozone trends in the easternmost U.S. (Figure 8b). A contributing factor to error in the simulated trends is that we apply country-wide scaling factors to the U.S. emissions for 2007 through 2010 and thus do not account for any changes in the geographic distribution of emissions in recent years.

One of the most pronounced features in Figures 7 and 8 is the east-west gradient in the U.S. ozone trends that develops during the summer months. While the percent decrease in NO_x emissions over our study period is similar across the country, the absolute decrease is larger in the eastern and Midwestern U.S. than in the west, leading to a greater reduction in NO_x concentrations in the eastern and Midwestern regions (Figure 9).

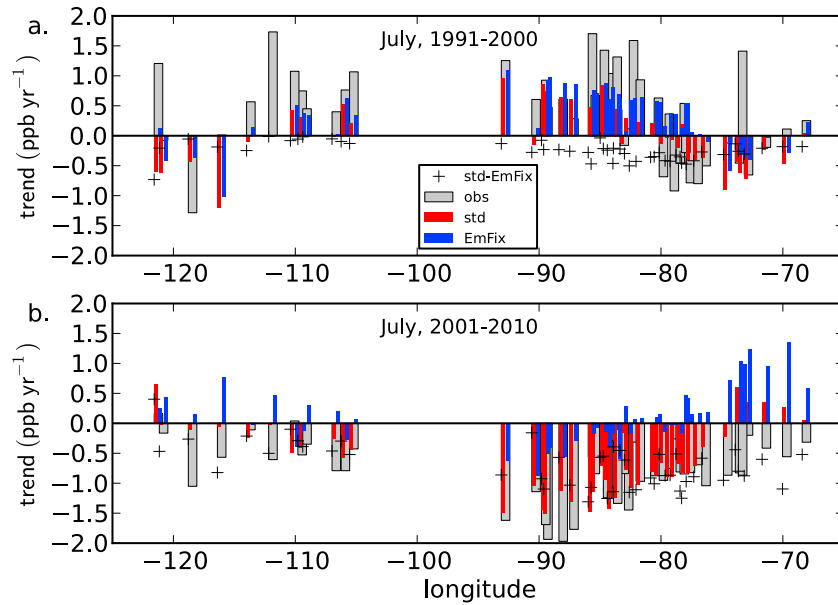


Figure 8. July trends in median daytime ozone at each site as a function of longitude for (a) 1991–2000 and (b) 2001–2010. Observed trends are in gray, trends from the standard simulation are in red, and trends from the EmFix simulation are in blue. The difference between the standard and EmFix simulation, representing the trend due to emission changes, is shown with cross signs.

Consequently, we next discuss the different drivers of trends in the eastern versus western U.S. We show regional trends for the 5th, 50th, and 95th percentiles in Table 2 in order to quantify the changes across the ozone distribution. We average within each region, construct the seasonal means from 2 month averages, and then calculate the regional trend.

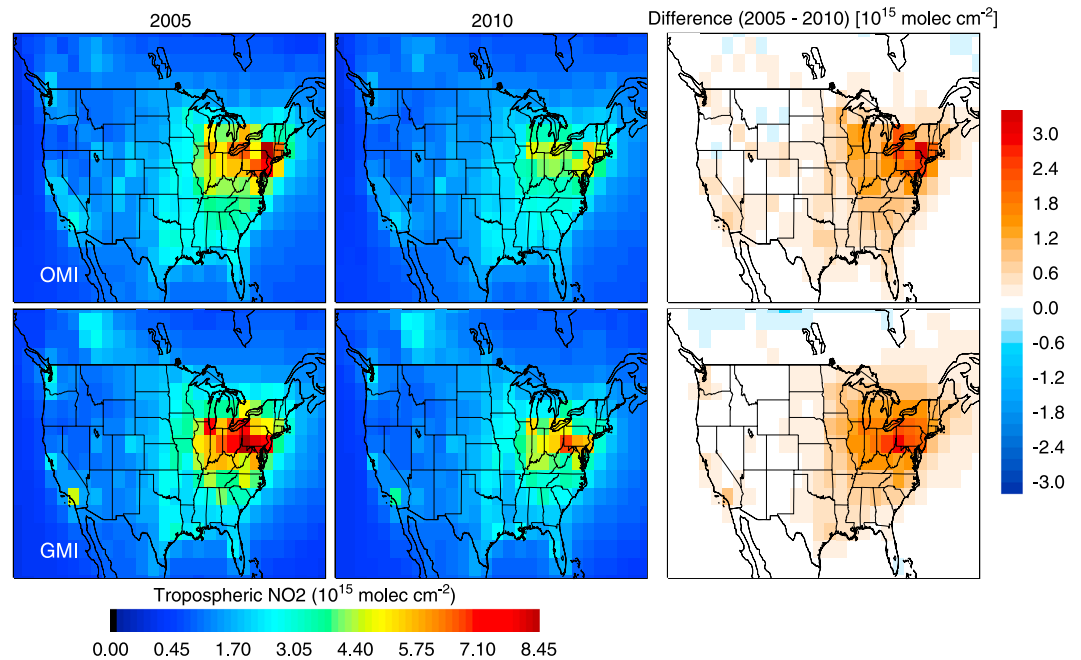


Figure 9. Tropospheric NO₂ columns from (top row) OMI and (bottom row) the standard GMI simulation for (left column) 2005, (center column) 2010, and (right column) the 2005–2010 differences. The simulated NO₂ is sampled at the OMI overpass time.

Table 2. Trend in Regionally Averaged 5th, 50th, and 95th Percentile Surface Ozone (ppbv yr⁻¹) for 1991–2010, With Statistically Significant Trends Indicated in Bold

Region	Obs/Model	Season			
		Jan/Feb	Mar/Apr	Jul/Aug	Oct/Nov
a. 5th Percentile					
New England	Obs	3.1E-1	1.7E-1	-3.0E-2	-7.1E-2
	Std	1.7E-1	1.1E-1	-2.2E-1	8.1E-3
	EmFix	-3.3E-2	7.9E-2	1.3E-2	-3.3E-3
Mid-Atlantic	Obs	4.1E-1	2.3E-1	-2.2E-1	5.7E-2
	Std	1.8E-1	1.0E-1	-3.0E-1	-1.8E-2
	EmFix	6.6E-2	1.1E-1	3.6E-2	-8.6E-3
Southeast	Obs	4.0E-1	2.0E-1	-2.9E-1	9.6E-2
	Std	3.1E-1	5.7E-2	-4.4E-1	3.8E-2
	EmFix	1.1E-1	3.0E-2	1.4E-1	-2.1E-2
Midwest	Obs	3.2E-1	3.0E-1	-1.8E-1	1.9E-1
	Std	2.5E-1	1.9E-1	-2.1E-1	7.8E-2
	EmFix	1.1E-1	1.4E-1	3.0E-2	4.4E-2
Mountain	Obs	1.2E-1	7.6E-2	1.4E-1	-4.6E-2
	Std	1.8E-1	4.7E-2	-7.8E-3	6.0E-2
	EmFix	6.2E-2	3.2E-2	1.2E-1	1.4E-2
California	Obs	1.4E-1	2.5E-1	-5.0E-2	-5.3E-2
	Std	1.4E-1	8.9E-2	3.7E-2	-5.7E-2
	EmFix	3.3E-2	3.5E-2	1.3E-1	-1.1E-1
b. 50th Percentile					
New England	Obs	9.4E-2	1.1E-1	-2.4E-1	-1.0E-1
	Std	1.2E-1	2.4E-2	-2.6E-1	-1.2E-2
	EmFix	-6.1E-2	6.8E-3	1.3E-1	-8.5E-3
Mid-Atlantic	Obs	2.1E-1	5.5E-2	-6.3E-1	3.2E-4
	Std	2.1E-1	2.6E-2	-5.1E-1	-6.1E-2
	EmFix	3.4E-2	5.4E-2	1.6E-1	-2.9E-2
Southeast	Obs	8.1E-2	-1.2E-2	-4.1E-1	-3.0E-2
	Std	2.1E-1	3.1E-2	-7.1E-1	-4.5E-2
	EmFix	2.3E-2	1.3E-1	1.2E-1	3.9E-3
Midwest	Obs	1.4E-1	7.1E-2	-4.8E-1	5.4E-2
	Std	3.3E-1	8.6E-2	-3.5E-1	1.6E-2
	EmFix	1.1E-1	5.2E-2	1.8E-1	-3.9E-3
Mountain	Obs	1.4E-1	1.3E-1	1.3E-1	-2.0E-2
	Std	1.5E-1	3.9E-2	-2.4E-2	1.1E-1
	EmFix	-7.5E-4	8.8E-3	1.6E-1	6.3E-2
California	Obs	8.5E-2	2.3E-1	-2.0E-1	-2.9E-1
	Std	6.9E-2	4.9E-2	-9.7E-2	-6.6E-2
	EmFix	-5.8E-2	-9.9E-3	1.1E-1	-8.6E-2
c. 95th Percentile					
New England	Obs	5.3E-2	4.6E-3	-7.5E-1	-2.3E-1
	Std	6.7E-2	-1.2E-1	-5.5E-1	-6.0E-2
	EmFix	-8.6E-2	6.1E-2	1.0E-1	4.8E-2
Mid-Atlantic	Obs	1.0E-2	-1.1E-1	-1.2E+0	-1.5E-1
	Std	9.4E-2	-1.3E-1	-6.8E-1	-1.0E-1
	EmFix	-5.1E-2	1.4E-1	2.7E-1	6.1E-2
Southeast	Obs	-1.5E-1	-8.2E-2	-6.9E-1	-1.3E-1
	Std	7.8E-2	-1.1E-1	-8.2E-1	6.6E-2
	EmFix	2.0E-2	2.3E-1	2.1E-1	3.8E-1
Midwest	Obs	-7.7E-2	-1.3E-1	-9.9E-1	-4.1E-3
	Std	1.7E-1	-1.5E-2	-4.9E-1	-4.2E-2
	EmFix	-2.0E-2	1.5E-1	3.0E-1	9.3E-2
Mountain	Obs	1.8E-1	1.8E-1	8.8E-2	-3.1E-2
	Std	1.3E-1	3.0E-2	-8.3E-2	7.4E-2
	EmFix	-2.8E-2	8.9E-3	1.7E-1	8.1E-2
California	Obs	-6.4E-2	-1.7E-2	-5.0E-1	-5.5E-1
	Std	-7.9E-2	2.9E-2	-2.7E-1	-1.8E-1
	EmFix	-2.5E-2	3.2E-2	4.1E-2	-9.6E-2

3.2.2. Trends in the Eastern and Midwestern U.S.

Significant positive trends are found in both the observations and the standard simulation at the 5th percentile (Table 2a) in the eastern and Midwest regions in January–February, although the simulation underestimates their magnitude. These trends are not present in the EmFix simulation, indicating that emissions are responsible for the trends. In the later years of the time series, the USIAV simulation (not shown) lies in between the EmFix and standard simulations, suggesting that these positive trends are due to a combination of increasing sources outside the U.S. and reduced ozone titration due to reductions in U.S. NO_x sources. Significant negative trends are present in the July/August observations at the 50th percentile for the Midwest, New England, and mid-Atlantic and at the 95th percentile for all regions except the Mountain West. The standard simulation also shows significant negative trends for most of these regions.

While the simulation shows a strong east-west gradient in the 50th and 95th percentile summer trends, it underestimates the magnitude of the negative 95th percentile trends in the eastern U.S., especially in the Ohio Valley region (Table 2c). This is consistent with the results of Zhou *et al.* [2013], which found that the Community Multiscale Air Quality model underestimated the simulated ozone decrease between 2002 and 2006 in the NO_x SIP Call region in part because the model underestimated the decrease in NO_x . Our standard simulation includes a 15% decrease in anthropogenic NO_x emissions from 2002 to 2006, smaller than the 20% and 33% decreases in ground-level and point emission sources, respectively, used in the Zhou *et al.*'s study. However, Figure 9 shows that the simulated decrease in NO_x from 2005 to 2010 is reasonable in this region. The negative trends in median ozone are also underestimated for the 2001–2010 period, and the standard simulation fails to capture the decreases in the easternmost sites (primarily in New England) in this period despite a large negative contribution from emissions (Figure 9b). This is due in part to meteorology making a large positive contribution to the trend at these sites, as shown by the EmFix simulation (Figure 3a), offsetting the effect of the emissions. Either the model overestimates this meteorological effect or underestimates the emission-induced changes in the northeastern U.S. Figure 9 suggests that the simulation places the largest NO_x decrease too far south.

3.2.3. Trends in the Western U.S.

Observed trends in the western U.S. show a less coherent pattern than those in the east (Figure 7). In the western U.S. during March–April, significant positive regional trends are present in the observations in California at the 5th and 50th percentiles but not in the Mountain West. However, the Mountain West shows significant positive trends in January–February in the observations and standard simulation. The standard simulation does not reproduce the positive trend in regionally averaged ozone in summer for the Mountain West, but we note that the observed trend is not statistically significant (Table 2). Dividing the trends by decade indicates that the positive western trends during summer occur in the first decade of the simulation (Figure 8). Although the emissions make a small negative contribution to the trend, both model simulations capture the sign of the positive trends west of 80°W, indicating that meteorology rather than emissions drives these trends in the early period (Figure 8a). Observations show high values for median ozone in the Southeast and Mountain West in 2000 (Figure 3), contributing to the positive trends for 1991–2000 west of 80°W.

There are several possible causes of the observed western trends and their underestimation by the hindcast. Skerlak *et al.* [2014] found that the mass flux into the planetary boundary layer from deep STT increased over the western U.S. from 1979 to 2011. Lin *et al.* [2015] found fewer stratospheric intrusions in the western U.S. for the two springs following the eruption of Mount Pinatubo in 1991, near the beginning of our study period. Here we explore the possible impact of changes in STT on surface ozone trends by examining the O3Strat tracer over the eastern and western U.S. for each month. We do not find any significant positive regional trends in O3Strat at the surface in either region. However, the 75th and 95th percentiles of the O3Strat tracer show a significant negative trend over the eastern U.S. in winter and spring, with the peak in O3Strat occurring in 1999 for both the eastern and western U.S. Figure S3 shows the O3Strat time series for April over the eastern U.S., which features a prominent peak in 1999 and a negative trend at high percentiles.

We also examine whether alternative emission time series can improve the simulated trends. Observations of NO_2 from OMI suggest that NO_x emissions for 2005–2006 over Asia may be underestimated [Lamsal *et al.*, 2010], and the growth of Asian NO_x emissions used in our standard simulation after 2006 is smaller than the change suggested by satellite observations [Lamsal *et al.*, 2011] and new bottom-up inventories [Zhao *et al.*, 2013]. Consequently, we conduct a sensitivity simulation for 2006–2010, scaling the NO_x emissions from

each grid box from the standard simulation based on scaling factors from OMI. The scaling factors are applied over the entire world. These scaling factors were derived using the approach of *Lamsal et al.* [2011] and yield NO_x emissions that are 15% higher over China and 5% higher globally in 2010 than the emissions used in the standard simulation. This simulation shows that the 1991–2010 trends in U.S. ozone are insensitive to this increase in Asian emissions. Indeed, Figure 8 shows that the positive trends observed in the western U.S. are primarily due to increases in the 1990s, so improved knowledge of emission trends in that decade would be important for improving our trend simulation.

Finally, we consider how robust the western U.S. trends are with respect to the choice of start date. Several of the western sites, including Yellowstone, Lassen, and the Grand Canyon, show pronounced increases between the 1991–1993 period and the post-1994 period. *Jaffe and Ray* [2007] note that the inlet height at several western national parks, including Yellowstone and Lassen, was raised in the mid-1990s. However, they did not find any systematic effects of the inlet height change on daytime ozone values. We investigate the effect of an increase in the early 1990s by calculating the observed trends in median ozone for 1995–2010. We find that excluding the first 4 years of data reduces the number of sites with significant positive trends from 5 to 1 in January, from 6 to 1 in March, from 4 to 3 in April, and from 3 to 0 in July and reduces the strength of the trends in most of these cases. Figure S4 shows the time series of deseasonalized monthly anomalies for the four sites that have statistically significant positive trends in January only when the first 4 years are included. The anomalies are calculated by removing the multiyear average monthly mean for each month. Evidently, the significant positive trends in the western U.S. appear to be heavily influenced by the first 4 years of our study period.

3.3. Changes in the Seasonal Cycle

The large decrease in surface ozone in summer compared to other seasons alters the observed seasonal cycle of ozone in the eastern U.S. [*Bloomer et al.*, 2010]. The peak baseline ozone concentrations in Europe now occur earlier in the year [*Parrish et al.*, 2013], and ozone over much of the U.S. now shows a broad spring/summer maximum [*Cooper et al.*, 2012], as was the case at rural sites in the late 1970s [*Logan*, 1989]. In the 1990s, a summer peak was present at the more polluted rural sites in the eastern U.S. such as Beltsville, MD, and ozone is highest in summer at these sites in the 2000s, albeit with lower values [*Bloomer et al.*, 2010; *Cooper et al.*, 2014].

Here we examine whether our simulations reproduce the observed changes in the amplitude and timing of the annual cycle. Since our simulated median ozone is biased high in most regions in summer (Table 1, Figure 2, and Figure S5), the simulations do not reproduce the summer ozone values seen in observations. However, the standard simulation shows a 6 ppbv decrease in median ozone for the eastern U.S. in summer for 2006–2010 compared to 1991–1994 and a 0.2 ppbv increase for the western U.S. for the same periods. This is in excellent agreement with the observed 1990–1994 versus 2006–2010 changes of -6 ppbv and 1 ppbv for the eastern and western U.S., respectively, reported by *Cooper et al.* [2012].

Figure 10 shows the change in the observed annual cycle of median daytime surface ozone for six regions of the U.S. shown in Figure 2 between the early (1992–1997) versus late (2005–2010) years of our study period. The annual cycle for each region is constructed by averaging together the median ozone from the sites within the region (Table S2). The same sites are included in both periods. The later period shows a reduction in the amplitude of the seasonal cycle in the mid-Atlantic and Midwest and to a lesser extent in the Southeast and California (Figure 10). This reduction is due primarily to lower summertime ozone in the later period, with a smaller contribution from increases in winter ozone. In the mid-Atlantic and Midwest regions, this leads to a broader spring through summer maxima in 2005–2010 rather than the pronounced summer peak seen in 1992–1997. The peak of the annual cycle in New England and the Southeast changes from May in the early period to April in the late period. The increase in winter ozone and decrease in summer ozone in New England is consistent with the results of *Clifton et al.* [2014]; for the northeastern U.S. changes in the Mountain West regions are small, with a slight increase in ozone in some months.

Figure 11 shows that the seasonality of the change between the two periods is well represented in the standard simulation in the four regions east of the Rocky Mountains, especially the mid-Atlantic and Midwest. The standard simulation captures the large decrease in summer, although the magnitude of the decrease is underestimated in the mid-Atlantic and Midwest and overestimated in the Southeast. We note, however, that

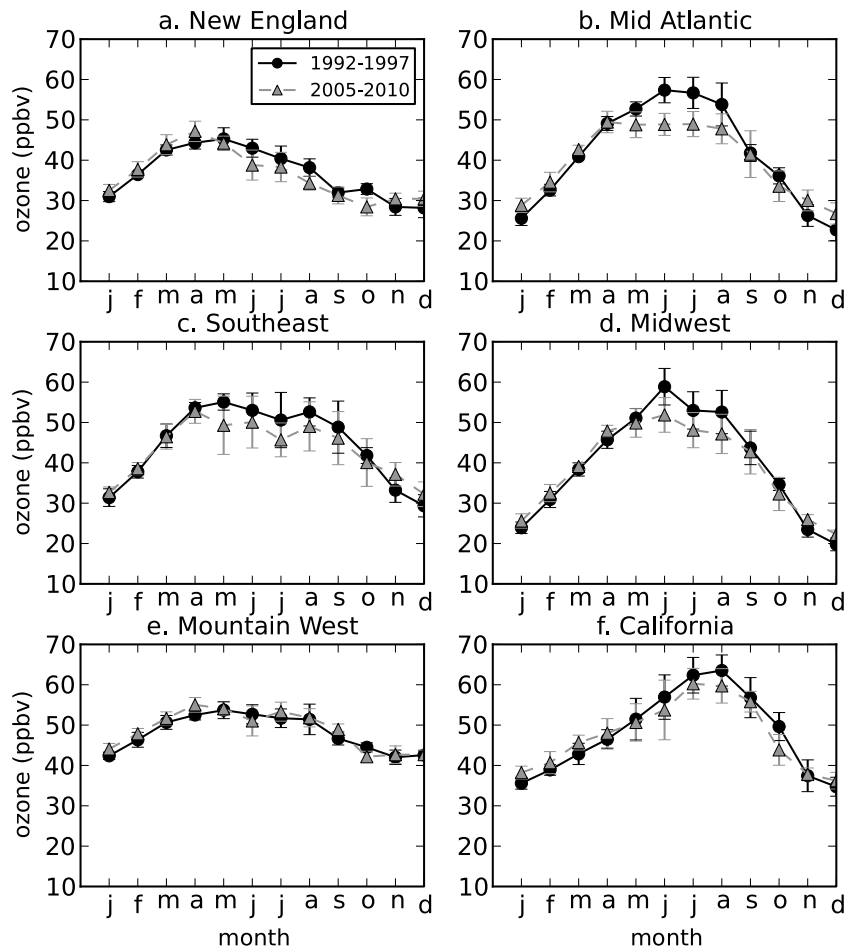


Figure 10. The annual cycle of observed median ozone averaged over 1992–1997 (black circles) and 2005–2010 (gray triangles) for each region. Error bars represent the standard deviation across years for each period. Region definitions are the same as in Figure 2.

the simulation also overestimates the amplitude of the seasonal cycle in the mid-Atlantic and places the peak ozone too late in the Midwest (Figure 2 and Figure S5). The amplitude of the seasonal cycle in the Southeast is overestimated in the early period (Figure S5). The standard simulation does not capture the large decreases in August and October ozone seen in California, and in the Mountain West it captures some but not all of the monthly changes.

The standard simulation captures the increases in winter and early spring, and the overall U-shape of the observed change in the annual cycle, for the four regions east of the Rocky Mountains (Figures 11a–11d). In contrast, the EmFix simulation does not capture this change in seasonality, instead showing an ozone increase in summer, indicating that emissions rather than meteorology are responsible for the change in the seasonal cycle. Similar features are evident at the 95th percentile as well (not shown). Comparison with the USIAV simulation indicates that both reduced ozone titration due to decreasing U.S. emissions and rising emissions outside the U.S. contribute to the winter increase in median ozone in the standard simulation for the eastern regions. Rising emissions outside the U.S. drive the winter increase in the California and Mountain West regions.

3.4. Changes in the Ozone-Temperature Relationship

Model studies predict that a warming climate will lead to increases in surface ozone, thus imposing a climate change penalty on air quality [Wu *et al.*, 2008]. Bloomer *et al.* [2009] used the observed slope of ozone versus temperature for several regions of the eastern U.S. to calculate this penalty for pre-2002 and post-2002 periods. They found that reductions in NO_x emissions led to a reduction in the penalty factor from approximately

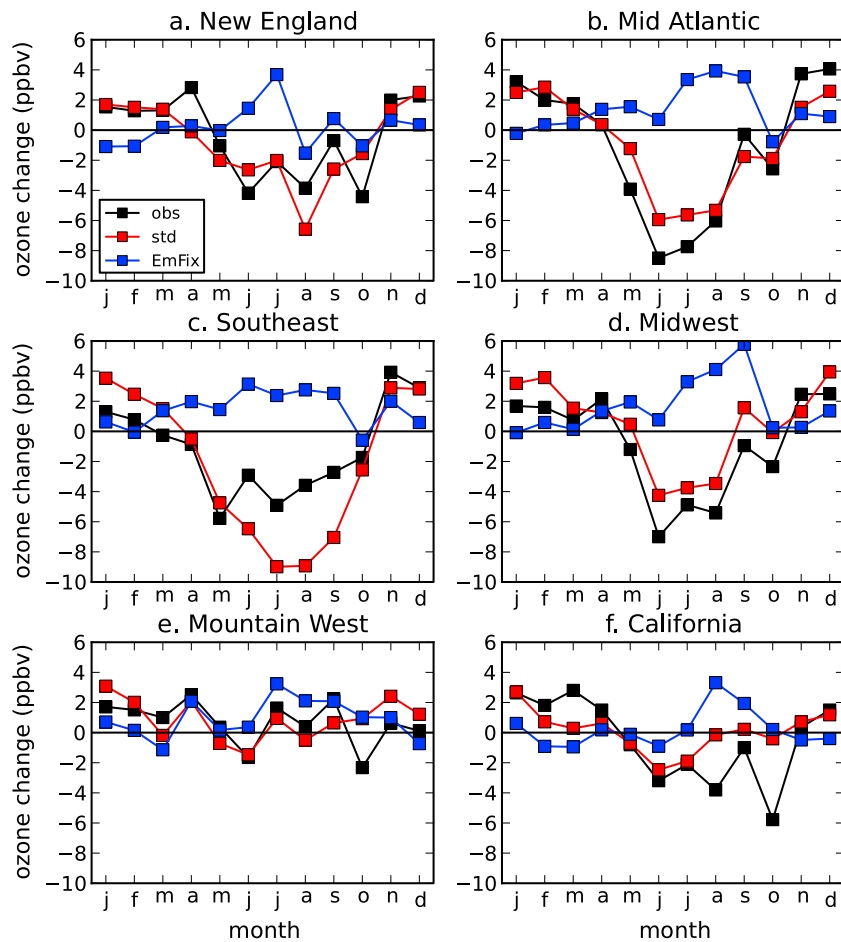


Figure 11. Regionally averaged change in median ozone between the 1992–1997 period and the 2005–2010 period for each month from observations (black), the standard simulation (red), and the EmFix simulation (blue). Region definitions are the same as in Figure 2.

3.2 to approximately 2.2 ppbv $O_3/^\circ C$. A modeling study by *Rasmussen et al.* [2012] also found a decrease in the slope of approximately 1 ppb K^{-1} for the same period. A study of three chemistry-climate models also found a greater increase in ozone with temperature over the 21st century at high NO_x levels for several regions of the northern hemisphere [*Doherty et al.*, 2013].

We examine whether our hindcast simulations reproduce the observed change in dO_3/dT before and after 2002. Following the approach of *Bloomer et al.* [2009], we bin the daytime ozone observations for May to September by temperature, aggregating together data from all selected sites in the region, and calculate the 5th, 25th, 50th, 75th, and 95th percentiles of the ozone distribution for each 3° temperature bin. We then calculate the slope of ozone versus temperature (dO_3/dT) for each percentile. The same process is applied to simulated ozone at the locations of the measurements.

Table 3 and Figure 12 present the observed and simulated slopes for the Great Lakes, mid-Atlantic, and Northeast regions of the U.S. for 1992–2002. The sites included in each region are listed in Table S2, and the region definitions for this analysis are chosen to follow the regions used by *Bloomer et al.* [2009]. Both the standard and EmFix simulations show good agreement with the observed slopes for the median, albeit with some underestimate in the mid-Atlantic. The simulations underestimate the observed slope at the 95th percentile but overestimate it at the 5th percentile (Table 3). Figure 12 also shows the change in dO_3/dT before and after 2002 (between 1992–2002 and 2003–2010). The standard simulation captures the observed decrease in the slope, while the EmFix simulation does not. This confirms that emission reductions rather than circulation changes drive the decrease in dO_3/dT after 2002.

Table 3. Observed and Simulated Slopes of May–September Daytime Ozone Versus Temperature (dO_3/dT) for the 5th, 25th, 50th, 75th, and 95th Percentile Ozone for Three Regions for the Period From 1992 to 2002 and the Change in Slope Between 1992–2002 and 2003–2010

%	Region	1992–2002 Slope ^a				Slope Change From 1992–2002 to 2003–2010 ^a			
		Obs	Std	EmFix	CCM	Obs	Std	EmFix	CCM
5th	Great Lakes ^b	1.85	2.13	2.19	1.62	−0.52	−0.69	−0.13	−0.60
	Mid-Atlantic ^c	2.28	2.45	2.36	0.96	−0.52	−1.10	−0.46	−0.90
	Northeast ^d	1.79	2.78	2.88	2.72	−0.11	−0.28	0.20	−0.48
25th	Great Lakes	2.09	2.09	2.12	1.39	−0.63	−0.71	−0.03	−0.14
	Mid-Atlantic	2.42	2.15	2.06	0.94	−0.75	−0.90	−0.18	−0.84
	Northeast	2.35	2.94	3.02	2.62	−0.37	−0.37	0.20	−0.56
50th	Great Lakes	2.27	2.16	2.17	1.67	−0.62	−0.71	0.01	−0.21
	Mid-Atlantic	2.56	2.03	1.98	0.95	−0.88	−0.77	−0.14	−0.82
	Northeast	2.70	2.88	2.88	2.36	−0.57	−0.44	0.25	−0.43
75th	Great Lakes	2.61	2.28	2.31	1.87	−0.80	−0.73	−0.10	−0.28
	Mid-Atlantic	3.03	2.02	1.98	1.03	−1.12	−0.70	0.005	−0.72
	Northeast	2.87	2.83	2.75	2.20	−0.75	−0.45	0.18	−0.41
95th	Great Lakes	2.86	2.20	2.24	1.94	−0.73	−0.69	−0.18	−0.27
	Mid-Atlantic	3.99	2.08	2.02	1.53	−1.55	−0.40	0.51	−1.22
	Northeast	3.24	2.78	2.73	2.21	−1.23	−0.62	0.14	−0.41

^aSlopes are in units of ppbv/degree C.

^bThe Great Lakes region includes the following sites: ALH157, PRK134, BVL130, SAL133, VIN140, OXF122, DCP114, LYK123, ANA115, UVL124.

^cThe mid-Atlantic includes the following sites: ESP127, SPD111, COW137, BLRI-RO, CDR119, PED108, PAR107, BEL116, WSP144.

^dThe Northeast region includes the following sites: LRL117, MKG113, ARE128, CTH110, WST109, ASH135.

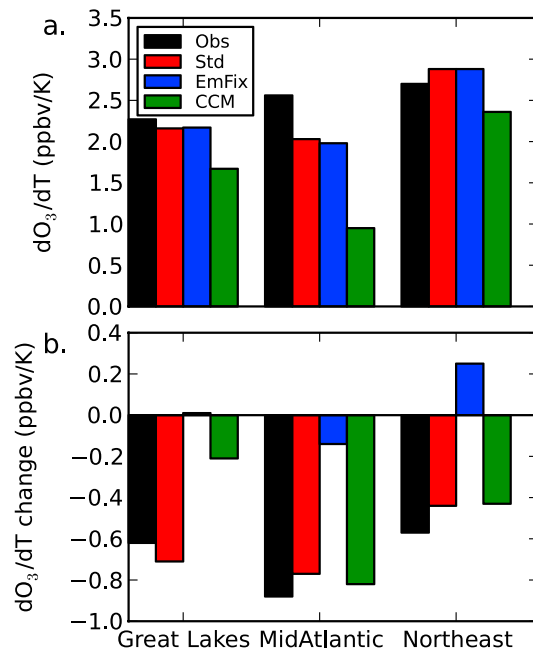


Figure 12. (a) The slope of median ozone with temperature (dO_3/dT) for 1992–2002 and (b) the change in slope from 1992–2002 to 2003–2010 for observations (black), the standard simulation (red), the EmFix simulation (blue), and the GEOSCCM simulation (green).

Our results suggest that the GMI CTM can simulate the impact of changing NO_x emissions on dO_3/dT over the last 20 years, an important capability for climate modeling studies. To see if this capability extends to CCM studies as well, we examine whether the GEOSCCM simulation reproduces the observed change in dO_3/dT . We bin the GEOSCCM-simulated ozone according to its simulated temperature. Schnell *et al.* [2014] found that the probability distribution of MDA8 O_3 differed depending on whether they treated their CTM simulation as a hindcast with sampling at the same time and place as the observations or sampled the model like a climate simulation with ozone sorted into percentiles independent of the observed ozone. Brown-Steiner *et al.* [2015] found that they better simulated the observed ozone versus temperature relationship at CASTNET sites in the post-SIP period when they ran their model as a general circulation model (GCM) rather than as a CTM with meteorology constrained by MERRA.

Table 3 shows that the GEOSCCM simulation underestimates dO_3/dT for 1992–2002 compared to both observations and the standard CTM simulation, especially in the mid-Atlantic. However, the change in slope between the two periods is

reasonable for the mid-Atlantic and Northeast (Figure 12). Based on a comparison with a MERRA-driven CTM simulation using the same emissions as the GEOSCCM, we conclude that the large differences in the mid-Atlantic in Figure 12a and the Great Lakes (Figure 12b) are due primarily to the MERRA versus free-running GCM difference, although the different emissions between the CCM simulation and our standard simulation also contribute. The lower values of dO_3/dT for the CCM than the CTM is consistent with the findings of *Brown-Steiner et al.* [2015]. While the ability of the GMI CTM and GEOSCCM to capture the reduction in dO_3/dT post-2002 is encouraging, we note that the relationship between ozone and temperature may change in a future climate due to factors such as changes in the position of the jet stream [Barnes and Fiore, 2013] and potentially different correlations between temperature and other aspects of meteorology in a changed climate.

4. Conclusions

We analyzed the observed IAV and trends in surface ozone over the United States for each season of 1991–2010 using the GMI CTM. The model IAV shows strong correlations with the observations for most sites in summer, but has weaker correlations in winter and spring, especially in the western U.S. The correlation between our standard simulation and the observed time series for regionally averaged July–August ozone is statistically significant in all regions, with correlation coefficients ranging from 0.46 to 0.89. IAV in summer ozone is related to meteorological variability in temperature, humidity, and stagnation, and these relationships are well captured by the CTM driven by MERRA meteorology. In contrast, IAV in winter ozone does not correlate strongly with temperature, so the use of realistic temperatures from MERRA does not lead to strong correlations between simulated and observed IAVs in winter. Variability in the contribution of stratospheric ozone to surface ozone appears to be a factor in the surface ozone IAV at some western sites in winter and spring.

Our standard hindcast simulation, driven by interannually varying fossil fuel and biomass burning emissions, reproduces the observed decrease in summertime ozone in the eastern U.S. and thus the reduction in the amplitude of the seasonal cycle. These features are not present in the hindcast driven by fixed emissions, confirming the role of precursor emission reductions in driving the summertime ozone reductions.

The standard simulation captures some of the observed positive trends in the western U.S. in winter but underestimates those trends in spring and summer. The underestimation of the summer trends is consistent with a previous hindcast study by *Koumoutsaris and Bey* [2012], who suggested that future hindcasts employ higher resolution, a coupled stratosphere, and improved regional emissions. We find that even with a coupled stratosphere and $1^\circ \times 1.25^\circ$ resolution, our hindcast cannot reproduce the magnitude of the western trends or the IAV at some western sites. While observations from OMI provide a space-based constraint on recent NO_x emissions, including OMI-based emissions did not resolve the discrepancy in the western trends. Instead, large ozone increases at the western sites in the early 1990s, seen in the observations but not the hindcast simulation, drive much of the statistical significance of these observed positive trends. Better understanding these early years is critical for reconciling hindcast simulations with observed trends in the western United States.

The hindcast reproduces well the change in dO_3/dT between the early years of the study period and the years after the NO_x SIP Call. The ability to simulate this shift and reproduce the east-west gradient in the trends, along with the significant correlations with the observed interannual variability at many sites, demonstrates the ability of a global model hindcast with MERRA meteorology to capture much of the regional ozone response to changes in emissions and meteorology. This capability is important for both hindcast simulations and model projections of future ozone concentrations.

References

- Allen, D., K. Pickering, B. Duncan, and M. Damon (2010), Impact of lightning NO emissions on North American photochemistry as determined using the Global Modeling Initiative (GMI) model, *J. Geophys. Res.*, *115*, D22301, doi:10.1029/2010JD014062.
- Ambrose, J. L., D. R. Reidmiller, and D. A. Jaffe (2011), Causes of high O_3 in the lower free troposphere over the Pacific Northwest as observed at the Mt. Bachelor Observatory, *Atmos. Environ.*, *45*(30), 5302–5315, doi:10.1016/j.atmosenv.2011.06.056.
- Arndt, D. S., M. O. Baringer, and M. R. Johnson (2010), State of the climate in 2009, *Bull. Am. Meteorol. Soc.*, *91*(7), s1–s222, doi:10.1175/BAMS-91-7-StateoftheClimate.
- Barnes, E. A., and A. M. Fiore (2013), Surface ozone variability and the jet position: Implications for projecting future air quality, *Geophys. Res. Lett.*, *40*, 2839–2844, doi:10.1002/grl.50411.
- Bloomer, B. J., J. W. Stehr, C. A. Piety, R. J. Salawitch, and R. R. Dickerson (2009), Observed relationships of ozone air pollution with temperature and emissions, *Geophys. Res. Lett.*, *36*, L09803, doi:10.1029/2009GL037308.

Acknowledgments

This work was supported by NASA's Modeling, Analysis, and Prediction program. The NASA High-End Computing Program provided resources to support this work through the NASA Center for Climate Simulation at Goddard Space Flight Center. GMI simulation results are available by request to Susan Strahan (susan.e.strahan@nasa.gov). EPA CASTNET data, OMI NO_2 data, and MERRA data are available at <http://epa.gov/castnet/javaweb/index.html>, http://disc.sci.gsfc.nasa.gov/Aura/data-holdings/OMI/omno2_v003.shtml, and <http://disc.sci.gsfc.nasa.gov/daac-bin/DataHoldings.pl>, respectively.

- Bloomer, B. J., K. Y. Vinnikov, and R. R. Dickerson (2010), Changes in seasonal and diurnal cycles of ozone and temperature in the eastern U.S., *Atmos. Environ.*, *44*(21–22), 2543–2551, doi:10.1016/j.atmosenv.2010.04.031.
- Brown-Steiner, B., P. G. Hess, and M. Y. Lin (2015), On the capabilities and limitations of GCM simulations of summertime regional air quality: A diagnostic analysis of ozone and temperature simulations in the US using CESM CAM-Chem, *Atmos. Environ.*, *101*, 134–148, doi:10.1016/j.atmosenv.2014.11.001.
- Bucsela, E. J., N. A. Krotkov, E. A. Celarier, L. N. Lamsal, W. H. Swartz, P. K. Bhartia, K. F. Boersma, J. P. Veefkind, J. F. Gleason, and K. E. Pickering (2013), A new stratospheric and tropospheric NO₂ retrieval algorithm for nadir-viewing satellite instruments: Applications to OMI, *Atmos. Meas. Tech.*, *6*(10), 2607–2626, doi:10.5194/amt-6-2607-2013.
- Butler, T. J., F. M. Vermeylen, M. Rury, G. E. Likens, B. Lee, G. E. Bowker, and L. McCluney (2011), Response of ozone and nitrate to stationary source NO_x emission reductions in the eastern USA, *Atmos. Environ.*, *45*(5), 1084–1094, doi:10.1016/j.atmosenv.2010.11.040.
- Camalier, L., W. Cox, and P. Dolwick (2007), The effects of meteorology on ozone in urban areas and their use in assessing ozone trends, *Atmos. Environ.*, *41*(33), 7127–7137, doi:10.1016/j.atmosenv.2007.04.061.
- Chan, E., and R. Vet (2010), Baseline levels and trends of ground level ozone in Canada and the United States, *Atmos. Chem. Phys.*, *10*(18), 8629–8647, doi:10.5194/acp-10-8629-2010.
- Clifton, O. E., A. M. Fiore, G. Correa, L. W. Horowitz, and V. Naik (2014), Twenty-first century reversal of the surface ozone seasonal cycle over the northeastern United States, *Geophys. Res. Lett.*, *41*, 7343–7350, doi:10.1002/2014GL061378.
- Cooper, O. R., et al. (2010), Increasing springtime ozone mixing ratios in the free troposphere over western North America, *Nature*, *463*(7279), 344–348, doi:10.1038/nature08708.
- Cooper, O. R., R. S. Gao, D. Tarasick, T. Leblanc, and C. Sweeney (2012), Long-term ozone trends at rural ozone monitoring sites across the United States, 1990–2010, *J. Geophys. Res.*, *117*, D22307, doi:10.1029/2012JD018261.
- Cooper, O. R., et al. (2014), Global distribution and trends of tropospheric ozone: An observation-based review, *Elem. Sci. Anthropocene*, *2*(1), 000029, doi:10.12952/journal.elementa.000029.
- Dentener, F., T. Keating, and H. Akimoto (Eds.) (2010), *Hemispheric Transport of Air Pollution, Part A: Ozone and Particulate Matter, Air Pollut. Stud. No. 17*, U. N., New York.
- Doherty, R., et al. (2013), Impacts of climate change on surface ozone and intercontinental ozone pollution: A multi-model study, *J. Geophys. Res. Atmos.*, *118*, 3744–3763, doi:10.1002/jgrd.50266.
- Duncan, B. N., R. V. Martin, A. C. Staudt, R. Yevich, and J. A. Logan (2003), Interannual and seasonal variability of biomass burning emissions constrained by satellite observations, *J. Geophys. Res.*, *108*(D2), 4040, doi:10.1029/2002JD002378.
- Duncan, B. N., S. E. Strahan, Y. Yoshida, S. D. Steenrod, and N. Livesey (2007), Model study of the cross-tropopause transport of biomass burning pollution, *Atmos. Chem. Phys.*, *7*(14), 3713–3736.
- Emery, C., J. Jung, N. Downey, J. Johnson, M. Jimenez, G. Yarwood, and R. Morris (2012), Regional and global modeling estimates of policy relevant background ozone over the United States, *Atmos. Environ.*, *47*, 206–217, doi:10.1016/j.atmosenv.2011.11.012.
- Environmental Protection Agency (EPA) (2001), Latest findings on national air quality: 2000 status and trends, EPA 454/K-01-002, Research Triangle Park, N. C.
- Environmental Protection Agency (EPA) (2006), *Air Quality Criteria for Ozone and Related Photochemical Oxidants, EPA 600/R-05/004aF*, vol. 1, EPA, Research Triangle Park, N. C.
- Environmental Protection Agency (EPA) (2011), Our nation's air: Status and trends through 2010, EPA-454/R-12-001, Research Triangle Park, N. C.
- Eyring, V., J.-F. Lamarque, P. Hess, F. Arfeuille, K. Bowman, M. P. Chipperfield, B. Duncan, A. Fiore, A. Gettelman, and M. A. Giorgetta (2013), Overview of IGAC/SPARC Chemistry-Climate Model Initiative (CCMI) community simulations in support of upcoming ozone and climate assessments, *Sparc Newsl.*, *40*, 48–66.
- Fiore, A. M., D. J. Jacob, I. Bey, R. M. Yantosca, B. D. Field, A. C. Fusco, and J. G. Wilkinson (2002), Background ozone over the United States in summer: Origin, trend, and contribution to pollution episodes, *J. Geophys. Res.*, *107*(D15), 4275, doi:10.1029/2001JD000982.
- Fiore, A. M., D. J. Jacob, H. Liu, R. M. Yantosca, T. D. Fairlie, and Q. Li (2003), Variability in surface ozone background over the United States: Implications for air quality policy, *J. Geophys. Res.*, *108*(D24), 4787, doi:10.1029/2003JD003855.
- Fiore, A. M., et al. (2009), Multimodel estimates of intercontinental source-receptor relationships for ozone pollution, *J. Geophys. Res.*, *114*, D04301, doi:10.1029/2008JD010816.
- Fiore, A. M., J. T. Oberman, M. Y. Lin, L. Zhang, O. E. Clifton, D. J. Jacob, V. Naik, L. W. Horowitz, J. P. Pinto, and G. P. Milly (2014), Estimating North American background ozone in U.S. surface air with two independent global models: Variability, uncertainties, and recommendations, *Atmos. Environ.*, *96*, 284–300.
- Frost, G. J., et al. (2006), Effects of changing power plant NO_x emissions on ozone in the eastern United States: Proof of concept, *J. Geophys. Res.*, *111*, D12306, doi:10.1029/2005JD006354.
- Gego, E., P. S. Porter, A. Gilliland, and S. T. Rao (2007), Observation-based assessment of the impact of nitrogen oxides emissions reductions on ozone air quality over the eastern United States, *J. Appl. Meteorol. Climatol.*, *46*(7), 994–1008, doi:10.1175/jam2523.1.
- Godowitch, J. M., C. Hogrefe, and S. T. Rao (2008), Diagnostic analyses of a regional air quality model: Changes in modeled processes affecting ozone and chemical-transport indicators from NO_x point source emission reductions, *J. Geophys. Res.*, *113*, D19303, doi:10.1029/2007JD009537.
- Guenther, A., B. Baugh, G. Brasseur, J. Greenberg, P. Harley, L. Klinger, D. Serca, and L. Vierling (1999), Isoprene emission estimates and uncertainties for the central African EXPRESSO study domain, *J. Geophys. Res.*, *104*(D23), 30,625–30,639, doi:10.1029/1999JD900391.
- Guenther, A., C. Geron, T. Pierce, B. Lamb, P. Harley, and R. Fall (2000), Natural emissions of non-methane volatile organic compounds; carbon monoxide, and oxides of nitrogen from North America, *Atmos. Environ.*, *34*(12–14), 2205–2230, doi:10.1016/s1352-2310(99)00465-3.
- Hegarty, J., H. Mao, and R. Talbot (2007), Synoptic controls on summertime surface ozone in the northeastern United States, *J. Geophys. Res.*, *112*, D14306, doi:10.1029/2006JD008170.
- Hess, P. G., and J.-F. Lamarque (2007), Ozone source attribution and its modulation by the Arctic oscillation during the spring months, *J. Geophys. Res.*, *112*, D11303, doi:10.1029/2006JD007557.
- Hogrefe, C., et al. (2011), An analysis of long-term regional-scale ozone simulations over the northeastern United States: Variability and trends, *Atmos. Chem. Phys.*, *11*(2), 567–582, doi:10.5194/acp-11-567-2011.
- Jacob, D. J., J. A. Logan, G. M. Gardner, R. M. Yevich, C. M. Spivakovsky, S. C. Wofsy, S. Sillman, and M. J. Prather (1993), Factors regulating ozone over the United States and its export to the global atmosphere, *J. Geophys. Res.*, *98*(D8), 14,817–14,826, doi:10.1029/98JD01224.
- Jaffe, D. (2011), Relationship between surface and free tropospheric ozone in the western U.S., *Environ. Sci. Technol.*, *45*(2), 432–438, doi:10.1021/es1028102.
- Jaffe, D., and J. Ray (2007), Increase in surface ozone at rural sites in the western US, *Atmos. Environ.*, *41*(26), 5452–5463, doi:10.1016/j.atmosenv.2007.02.034.

- Jaffe, D., H. Price, D. Parrish, A. Goldstein, and J. Harris (2003), Increasing background ozone during spring on the west coast of North America, *Geophys. Res. Lett.*, *30*(12), 1613, doi:10.1029/2003GL017024.
- Kalnay, E., et al. (1996), The NCEP/NCAR 40-year reanalysis project, *Bull. Am. Meteorol. Soc.*, *77*, 437–471.
- Kim, S. W., A. Heckel, S. A. McKeen, G. J. Frost, E. Y. Hsie, M. K. Trainer, A. Richter, J. P. Burrows, S. E. Peckham, and G. A. Grell (2006), Satellite-observed US power plant NO_x emission reductions and their impact on air quality, *Geophys. Res. Lett.*, *33*, L22812, doi:10.1029/2006GL027749.
- Koumoutsaris, S., and I. Bey (2012), Can a global model reproduce observed trends in summertime surface ozone levels?, *Atmos. Chem. Phys.*, *12*(15), 6983–6998, doi:10.5194/acp-12-6983-2012.
- Kuhns, H., E. M. Knipping, and J. M. Vukovich (2005), Development of a United States-Mexico emissions inventory for the Big Bend Regional Aerosol and Visibility Observational (BRAVO) study, *J. Air Waste Manage.*, *55*(5), 677–692.
- Lamsal, L. N., R. V. Martin, A. van Donkelaar, E. A. Celarier, E. J. Bucsela, K. F. Boersma, R. Dirksen, C. Luo, and Y. Wang (2010), Indirect validation of tropospheric nitrogen dioxide retrieved from the OMI satellite instrument: Insight into the seasonal variation of nitrogen oxides at northern midlatitudes, *J. Geophys. Res.*, *115*, D05302, doi:10.1029/2009JD013351.
- Lamsal, L. N., R. V. Martin, A. Padmanabhan, A. van Donkelaar, Q. Zhang, C. E. Sioris, K. Chance, T. P. Kurosu, and M. J. Newchurch (2011), Application of satellite observations for timely updates to global anthropogenic NO_x emission inventories, *Geophys. Res. Lett.*, *38*, L05810, doi:10.1029/2010GL046476.
- Lamsal, L. N., et al. (2014), Evaluation of OMI operational standard NO₂ column retrievals using in situ and surface-based NO₂ observations, *Atmos. Chem. Phys. Discuss.*, *14*(10), 14,519–14,573, doi:10.5194/acpd-14-14519-2014.
- Langford, A. O., K. C. Aikin, C. S. Eubank, and E. J. Williams (2009), Stratospheric contribution to high surface ozone in Colorado during springtime, *Geophys. Res. Lett.*, *36*, L12801, doi:10.1029/2009GL038367.
- Langford, A. O., J. Brioude, O. R. Cooper, C. J. Senff, R. J. Alvarez, R. M. Hardesty, B. J. Johnson, and S. J. Oltmans (2012), Stratospheric influence on surface ozone in the Los Angeles area during late spring and early summer of 2010, *J. Geophys. Res.*, *117*, D00V06, doi:10.1029/2011JD016766.
- Langford, A. O., et al. (2015), An overview of the 2013 Las Vegas Ozone Study (LVOS): Impact of stratospheric intrusions and long-range transport on surface air quality, *Atmos. Environ.*, doi:10.1016/j.atmosenv.2014.08.040.
- Lefohn, A., and J. Foley (1993), Establishing relevant ozone standards to protect vegetation and human health: Exposure dose-response considerations, *J. Air Waste Manage.*, *43*(1), 106–112.
- Lefohn, A. S., D. Shadwick, and S. J. Oltmans (2010), Characterizing changes in surface ozone levels in metropolitan and rural areas in the United States for 1980–2008 and 1994–2008, *Atmos. Environ.*, *44*(39), 5199–5210, doi:10.1016/j.atmosenv.2010.08.049.
- Lefohn, A. S., H. Wernli, D. Shadwick, S. Limbach, S. J. Oltmans, and M. Shapiro (2011), The importance of stratospheric-tropospheric transport in affecting surface ozone concentrations in the western and northern tier of the United States, *Atmos. Environ.*, *45*(28), 4845–4857, doi:10.1016/j.atmosenv.2011.06.014.
- Lefohn, A. S., H. Wernli, D. Shadwick, S. J. Oltmans, and M. Shapiro (2012), Quantifying the importance of stratospheric-tropospheric transport on surface ozone concentrations at high- and low-elevation monitoring sites in the United States, *Atmos. Environ.*, *62*, 646–656, doi:10.1016/j.atmosenv.2012.09.004.
- Leibensperger, E. M., L. J. Mickley, and D. J. Jacob (2008), Sensitivity of US air quality to mid-latitude cyclone frequency and implications of 1980–2006 climate change, *Atmos. Chem. Phys.*, *8*, 7075–7086.
- Levelt, P. F., E. Hilsenrath, G. W. Leppelmeier, G. H. J. van den Oord, P. K. Bhartia, J. Tamminen, J. F. de Haan, and J. P. Veefkind (2006), Science objectives of the Ozone Monitoring Instrument, *IEEE Trans. Geosci. Remote Sens.*, *44*(5), 1199–1208, doi:10.1109/tgrs.2006.872336.
- Lin, C. Y. C., D. J. Jacob, J. W. Munger, and A. M. Fiore (2000), Increasing background ozone in surface air over the United States, *Geophys. Res. Lett.*, *27*(21), 3465–3468, doi:10.1029/2000GL011762.
- Lin, M., A. M. Fiore, O. R. Cooper, L. W. Horowitz, A. O. Langford, H. Levy, B. J. Johnson, V. Naik, S. J. Oltmans, and C. J. Senff (2012), Springtime high surface ozone events over the western United States: Quantifying the role of stratospheric intrusions, *J. Geophys. Res.*, *117*, D00V22, doi:10.1029/2012JD018151.
- Lin, M., A. M. Fiore, L. W. Horowitz, A. O. Langford, S. J. Oltmans, D. Tarasick, and H. E. Reider (2015), Climate variability modulates western U.S. ozone air quality in spring via deep stratospheric intrusions, *Nat. Commun.*, *6*, 7105, doi:10.1038/ncomms8105.
- Lippmann, M. (1989), Health effects of ozone: A critical review, *J. Air Waste Manage.*, *39*(5), 672–695.
- Logan, J. A. (1989), Ozone in rural areas of the United States, *J. Geophys. Res.*, *94*(D6), 8511–8532, doi:10.1029/JD094iD06p08511.
- Ohara, T., H. Akimoto, J. Kurokawa, N. Horii, K. Yamaji, X. Yan, and T. Hayasaka (2007), An Asian emission inventory of anthropogenic emission sources for the period 1980–2020, *Atmos. Chem. Phys.*, *7*(16), 4419–4444.
- Olivier, J. G., J. A. Van Aardenne, F. J. Dentener, V. Pagliari, L. N. Ganzeveld, and J. A. Peters (2005), Recent trends in global greenhouse gas emissions: Regional trends 1970–2000 and spatial distribution of key sources in 2000, *Environ. Sci.*, *2*(2–3), 81–99.
- Oltmans, S. J., et al. (2013), Recent tropospheric ozone changes—A pattern dominated by slow or no growth, *Atmos. Environ.*, *67*, 331–351, doi:10.1016/j.atmosenv.2012.10.057.
- Oman, L. D., J. R. Ziemke, A. R. Douglass, D. W. Waugh, C. Lang, J. M. Rodriguez, and J. E. Nielsen (2011), The response of tropical tropospheric ozone to ENSO, *Geophys. Res. Lett.*, *38*, L13706, doi:10.1029/2011GL047865.
- Parrish, D. D., et al. (2004), Changes in the photochemical environment of the temperate North Pacific troposphere in response to increased Asian emissions, *J. Geophys. Res.*, *109*, D23S18, doi:10.1029/2004JD004978.
- Parrish, D. D., D. B. Millet, and A. H. Goldstein (2009), Increasing ozone in marine boundary layer inflow at the west coasts of North America and Europe, *Atmos. Chem. Phys.*, *9*(4), 1303–1323.
- Parrish, D. D., et al. (2012), Long-term changes in lower tropospheric baseline ozone concentrations at northern mid-latitudes, *Atmos. Chem. Phys.*, *12*(23), 11,485–11,504, doi:10.5194/acp-12-11485-2012.
- Parrish, D. D., et al. (2013), Lower tropospheric ozone at northern midlatitudes: Changing seasonal cycle, *Geophys. Res. Lett.*, *40*, 1631–1636, doi:10.1002/grl.50303.
- Pozzoli, L., G. Janssens-Maenhout, T. Diehl, I. Bey, M. G. Schultz, J. Feichter, E. Vignati, and F. Dentener (2011), Re-analysis of tropospheric sulfate aerosol and ozone for the period 1980–2005 using the aerosol-chemistry-climate model ECHAM5-HAMMOZ, *Atmos. Chem. Phys.*, *11*(18), 9563–9594.
- Prather, M. J., X. Zhu, Q. Tang, J. N. Hsu, and J. L. Neu (2011), An atmospheric chemist in search of the tropopause, *J. Geophys. Res.*, *116*, D04306, doi:10.1029/2010JD014939.
- Rasmussen, D. J., A. M. Fiore, V. Naik, L. W. Horowitz, S. J. McGinnis, and M. G. Schultz (2012), Surface ozone-temperature relationships in the eastern US: A monthly climatology for evaluating chemistry-climate models, *Atmos. Environ.*, *47*, 142–153, doi:10.1016/j.atmosenv.2011.11.021.
- Rastigejev, Y., R. Park, M. P. Brenner, and D. J. Jacob (2010), Resolving intercontinental pollution plumes in global models of atmospheric transport, *J. Geophys. Res.*, *115*, D02302, doi:10.1029/2009JD012568.

- Rienecker, M. M., et al. (2011), MERRA: NASA's Modern-Era Retrospective Analysis for Research and Applications, *J. Clim.*, *24*(14), 3624–3648, doi:10.1175/JCLI-D-11-00015.1.
- Schnell, J. L., C. D. Holmes, A. Jangam, and M. J. Prather (2014), Skill in forecasting extreme ozone pollution episodes with a global atmospheric chemistry model, *Atmos. Chem. Phys.*, *14*(15), 7721–7739, doi:10.5194/acp-14-7721-2014.
- Schoeberl, M. R., et al. (2006), Overview of the EOS Aura mission, *IEEE Trans. Geosci. Remote Sens.*, *44*(5), 1066–1074, doi:10.1109/tgrs.2005.861950.
- Seaman, N. L., and S. A. Michelson (2000), Mesoscale meteorological structure of a high-ozone episode during the 1995 NARSTO-Northeast study, *J. Appl. Meteorol.*, *39*(3), 384–398, doi:10.1175/1520-0450(2000)039<0384:mmsoah>2.0.co;2.
- Sillman, S., and P. J. Samson (1995), Impact of temperature on oxidant photochemistry in urban, polluted rural and remote environments, *J. Geophys. Res.*, *100*(D6), 11,497–11,508, doi:10.1029/94JD02146.
- Simon, H., A. Reff, B. Wells, J. Xing, and N. Frank (2015), Ozone trends across the United States over a period of decreasing NO_x and VOC emissions, *Environ. Sci. Technol.*, *49*, 186–195, doi:10.1021/es504514z.
- Skerlak, B., M. Sprenger, and H. Wernli (2014), A global climatology of stratosphere-troposphere exchange using the ERA-Interim data set from 1979 to 2011, *Atmos. Chem. Phys.*, *14*(2), 913–937, doi:10.5194/acp-14-913-2014.
- Sprenger, M., and H. Wernli (2003), A northern hemispheric climatology of cross-tropopause exchange for the ERA15 time period (1979–1993), *J. Geophys. Res.*, *108*(D12), 8521, doi:10.1029/2002JD002636.
- Strahan, S. E., B. N. Duncan, and P. Hoor (2007), Observationally derived transport diagnostics for the lowermost stratosphere and their application to the GMI chemistry and transport model, *Atmos. Chem. Phys.*, *7*(9), 2435–2445.
- Strahan, S. E., A. R. Douglass, and P. A. Newman (2013), The contributions of chemistry and transport to low arctic ozone in March 2011 derived from Aura MLS observations, *J. Geophys. Res. Atmos.*, *118*, 1563–1576, doi:10.1002/jgrd.50181.
- Tong, D. Q., and D. L. Mauzerall (2006), Spatial variability of summertime tropospheric ozone over the continental United States: Implications of an evaluation of the CMAQ model, *Atmos. Environ.*, *40*(17), 3041–3056, doi:10.1016/j.atmosenv.2005.11.058.
- van der Werf, G. R., J. T. Randerson, L. Giglio, G. J. Collatz, M. Mu, P. S. Kasibhatla, D. C. Morton, R. S. DeFries, Y. Jin, and T. T. van Leeuwen (2010), Global fire emissions and the contribution of deforestation, savanna, forest, agricultural, and peat fires (1997–2009), *Atmos. Chem. Phys.*, *10*(23), 11,707–11,735, doi:10.5194/acp-10-11707-2010.
- van Donkelaar, A., et al. (2008), Analysis of aircraft and satellite measurements from the Intercontinental Chemical Transport Experiment (INTEX-B) to quantify long-range transport of East Asian sulfur to Canada, *Atmos. Chem. Phys.*, *8*(11), 2999–3014.
- Vingarzan, R. (2004), A review of surface ozone background levels and trends, *Atmos. Environ.*, *38*(21), 3431–3442, doi:10.1016/j.atmosenv.2004.03.030.
- Wang, J., and J. Angell (1999), Air Stagnation Climatology for the United States (1948–1998), NOAA/Air Resour. Lab. [Available at <http://www.arl.noaa.gov/documents/reports/atlas.pdf>.]
- Wise, E. K., and A. C. Comrie (2005), Meteorologically adjusted urban air quality trends in the southwestern United States, *Atmos. Environ.*, *39*(16), 2969–2980, doi:10.1016/j.atmosenv.2005.01.024.
- Wu, S., L. Mickley, E. Leibensperger, D. Jacob, D. Rind, and D. Streets (2008), Effects of 2000–2050 global change on ozone air quality in the United States, *J. Geophys. Res.*, *113*, D06302, doi:10.1029/2007JD008917.
- Yienger, J. J., and H. Levy (1995), Empirical-model of global soil-biogenic NO_x emissions, *J. Geophys. Res.*, *100*(D6), 11,447–11,464, doi:10.1029/95JD00370.
- Zeng, G., and J. A. Pyle (2005), Influence of El Niño Southern Oscillation on stratosphere/troposphere exchange and the global tropospheric ozone budget, *Geophys. Res. Lett.*, *32*, L01814, doi:10.1029/2004GL021353.
- Zhang, L., D. J. Jacob, N. V. Downey, D. A. Wood, D. Blewitt, C. C. Carouge, A. van Donkelaar, D. B. A. Jones, L. T. Murray, and Y. X. Wang (2011), Improved estimate of the policy-relevant background ozone in the United States using the GEOS-Chem global model with 1/2 degrees × 2/3 degrees horizontal resolution over North America, *Atmos. Environ.*, *45*(37), 6769–6776, doi:10.1016/j.atmosenv.2011.07.054.
- Zhang, L., D. J. Jacob, X. Yue, N. V. Downey, D. A. Wood, and D. Blewitt (2014), Sources contributing to background surface ozone in the US Intermountain West, *Atmos. Chem. Phys.*, *14*(11), 5295–5309, doi:10.5194/acp-14-5295-2014.
- Zhang, Q., et al. (2009), Asian emissions in 2006 for the NASA INTEX-B mission, *Atmos. Chem. Phys.*, *9*(14), 5131–5153.
- Zhao, B., S. X. Wang, H. Liu, J. Y. Xu, K. Fu, Z. Klimont, J. M. Hao, K. B. He, J. Cofala, and M. Amann (2013), NO_x emissions in China: Historical trends and future perspectives, *Atmos. Chem. Phys.*, *13*(19), 9869–9897, doi:10.5194/acp-13-9869-2013.
- Zhou, W., D. S. Cohan, and S. L. Napelenok (2013), Reconciling NO_x emissions reductions and ozone trends in the U.S., 2002–2006, *Atmos. Environ.*, *70*, 236–244, doi:10.1016/j.atmosenv.2012.12.038.